# Facies and provenance analysis of the Midcontinent Rift System (MRS) in Kansas

by

Iffat Azmi

B.S., University of Dhaka, 2014
M.S., University of Dhaka, 2015

A THESIS

submitted in partial fulfillment of the requirements for the degree

MASTER OF SCIENCE

Department of Geology
College of Arts and Sciences

KANSAS STATE UNIVERSITY
Manhattan, Kansas

2020

Approved by:

Major Professor
Dr. Karin Goldberg

# Copyright

# Abstract

The Midcontinent Rift System (MRS) formed a half-graben that extends into NE Kansas. The Precambrian rift succession, penetrated by Texaco Noel Poersch#1 (NP#1) well in Washington Co. at depths between 2846 and 11300 ft, comprises two successions. The lower one (11300-7429 ft) is dominated by clastic sediments and the upper one (7429-2846 ft) mainly by volcanic rocks, which suggests a radical change during rift evolution. This study is aimed at describing the sedimentary succession within the rift in Kansas, relating variations in sedimentary facies to the different stages of rift development. Detailed facies and provenance analyses were carried out in discontinuous cores retrieved from the lower and upper successions (5395-11300 ft deep). Sixteen lithofacies were identified, grouped into six different facies associations (fluvial, eolian, mudflat/lake margin, lacustrine, alluvial fan, and fan delta). Overall, the studied succession comprises continental deposits laid down dominantly in alluvial and eolian settings, with the intermittent development of lacustrine systems. Three rift sequences, bound by flooding surfaces and controlled by tectonic pulses in rift basin, were identified. Superimposed on the tectonic phases, changing climate conditions resulted in recurrent dry and wet cycles. Provenance analysis showed a higher contribution of infracrustal rocks in the source areas. Minor shifts in provenance could be due to re-arrangements of faulted block and variable proportion of axial vs. transversal input into the rift basin. Despite the tectono-stratigraphic framework typical of a syn-rift succession, based on the available geochronological and compositional data, the rift succession in KS seems to be more compatible with post-rift successions elsewhere.

# Table of Contents


List of Figures ..... vi

List of Tables ..... ix

Acknowledgements ..... x

Chapter 1 - Introduction ..... 1

Chapter 2 - Geologic background ..... 4

2.1 Identification of the rift and its structure in Kansas ..... 4

2.2 Sedimentology of the rift ..... 6

Chapter 3 - Methods of investigation ..... 13

3.1 Core description and facies analysis ..... 13

3.2 Quantitative petrographic analysis ..... 15

Chapter 4 - Results and interpretations ..... 22

4.1 Facies analysis ..... 22

4.1.1 Core description and facies identification ..... 22

4.1.2 Facies associations and depositional environments ..... 28

4.1.2.1 Eolian Facies Association ..... 28

4.1.2.2 Fluvial Facies Association ..... 30

4.1.2.3 Lacustrine Facies Association ..... 30

4.1.2.4 Mudflat/ lake margin Facies Association ..... 31

4.1.2.5 Fan delta Facies Association ..... 31

4.1.2.6 Alluvial fan Facies Association ..... 32

4.2 Provenance analysis ..... 34

4.2.1 Quantitative petrographic analysis ..... 34

4.2.2 Provenance analysis and interpretation ..... 46

Chapter 5 - Discussion ..... 48

5.1 Depositional model ..... 48

5.2 Stratigraphic framework ..... 57

5.3 Correlation with other parts of MRS ..... 61

Chapter 6 - Conclusion ........................................................................................................ 65
References.................................................................................................................. 67
Appendix A................................................................................................................ 71
Appendix B................................................................................................................ 72

# List of Figures


Figure 1.1 : Gravity anomaly map showing the regional extent of the MRS (Stein et al., 2018). . 2

Figure 1.2 : Residual Bouger gravity map of Kansas, the second-order regional trend removed (after Xia et al., 1996). ........ 3

Figure 2.1 : Proposed model for the MRS basin structure and bounding faults in KS. ........ 5

Figure 2.2 : Lithostratigraphic column of MRS basin fill from Upper Michigan (modified from Ojakangas and Dickas, 2002). ........ 9

Figure 2.3 : Location map of the Midcontinent Rift System showing the rift segment in KS with the approximate location of the Noel Poersch (NP#1). Extracted from “Mineral deposits of the Midcontinent Rift System” https://www.arcgis.com/apps/MapSeries/index.html?appid=6687aedec0c2452db15b85ea253fb842). ........ 11

Figure 2.4 : Wireline log of Noel Poersch#1, KS, showing the eleven core intervals used in this study (modified from Berendsen, 1997). ........ 12

Figure 3.1 : Sandstone classification after McBride (1963) ........ 18

Figure 3.2 : Ternary plots of sandstone composition for provenance analysis (after Dickinson, 1985); refer to Table-3.2 for key. ........ 19

Figure 4.1 : Facies table with description and interpretation of the sixteen facies identified on the studied cores. ........ 22

Figure 4.2 : Distribution of the identified lithofacies in the cores from NP#1. The colors in the bars adjacent to the core photographs correspond to the facies in Figure 4.1 (except for magenta, representing volcanic rocks). ........ 23

Figure 4.3 : Representative photos of the facies identified in the studied cores. ........ 24

Figure 4.4 : Overall abundance (calculated as percentage over total thickness) of the identified facies in cores from NP#1. ........ 25

Figure 4.5 : Facies distribution within different sections for cores from NP#1. ........ 27

Figure 4.6 : Description and interpretation of the established facies associations. ........ 29

Figure 4.7 : Integrated sedimentary log, with the distribution of facies associations and vertical facies successions. ........ 33

Figure 4.8 : Nomenclature used for mixtures of gravel, sand, and mud in sedimentary rocks (after Nichols, 2006), and the distribution of analyzed samples. .................................................. 34
Figure 4.9 : Textures and structures of the quantified samples, A- very coarse- coarse, poorly-sorted sandstone; NP1 9170 feet; plane polarized light (PP), B- bimodal, fine-coarse poorly sorted sandstone; NP1 11295 feet, crossed polarizers (XP), C- medium, well-sorted sandstone; NP1 8056.6 feet; XP, D- laminated siltstone with fine sandstone interbeds; NP1 7153 feet; PP, E- low-angle cross stratification; NP1 11290 feet; XP, and F- low-angle cross lamination with inverse grading (inverted triangles); NP1 11296 feet; XP......................... 35
Figure 4.10 : Detrital composition of the samples in NP#1 plotted in McBride (1963) diagram (Q- quartz, F- feldspar and L- lithics)...................................................................... 36
Figure 4.11 : Composition of the quantified samples, A- Lithic arkose; NP1 11290 feet; Section A; crossed polarizers (XP), B- Lithic arkose; NP1 10509 feet; Section B; XP, C- Feldspathic litharenite; NP1 7568 feet; Section C; XP, D- Feldspathic litharenite; NP1 7152 feet; Section D; XP, E- Arkose; NP1 8480 feet; Section D; XP, F- Arkose; NP1 5396 feet; Section E; XP......................................................................................................... 38
Figure 4.12 : Diagenetic constituents identified in thin sections from NP#1; A- Albite overgrowths covering feldspars; NP1 11063.5; Section A; XP, B- Albite replacing orthoclase; NP1 11296; Section A; XP, C- Calcite filling intergranular pores and replacing albite overgrowths; NP1 10515; Section B; XP, D- Coarsely-crystalline calcite in rock fracture; NP1 9164.7; Section B; XP, E- Ferroan calcite replacing diagenetic silica in rock fracture; NP1 11295; Section A; PP, F- Calcite filling fenestrae lined with zeolite; NP1 5404.2; Section E; XP.............................................................................................. 44
Figure 4.13 : Diagenetic constituents identified on thin sections from NP#1; A- Illite cement, lining detrital grains and filling the pores; NP1 10510; Section B; XP, B- Iron oxide/hydroxide replacing detrital matrix and illite; NP1 7154.2; Section E; XP, C- Microcrystalline titanium mineral filling intergranular pores; NP1 7154; Section E; XP, D- Prismatic epidote replacing other diagenetic constituents; NP1 7154.2; Section E; XP, E and F- Vermicular chlorite engulfed by diagenetic silica in rock fracture; NP1 11061; Section A; XP and PP, respectively......................................................................... 45
Figure 4.14 : Distribution of the studied samples in the provenance Dickinson I diagram (Dickinson, 1985). ........................................................................................... 47

Figure 5.1 : Depositional model proposed for Section A. The red star marks the approximate location of NP#1 well. ........ 50
Figure 5.2 : Depositional model proposed for Section B-1. The red star marks the approximate location of NP#1 well. ........ 52
Figure 5.3 : Depositional model proposed for Section B-2. The red star marks the approximate location of NP#1 well. ........ 53
Figure 5.4 : Depositional model proposed for Section C. The red star marks the approximate location of NP#1 well. ........ 55
Figure 5.5 : Depositional model proposed for Section D. The red star marks the approximate location of NP#1 well. ........ 55
Figure 5.6 : Integrated sedimentary log with identified sequence of rift basin fill within NP#1. 59
Figure 5.7 : Comparative stratigraphy of units that comprise the Keeweenawan Supergroup in different locations. Age data and stratigraphic nomenclature for the different locations compiled from Berendsen, 1997 (NP#1 KS), Anderson et al., 1987 (IA) and Ojakangas et al., 2002. ........ 62
Figure 5.8 : Compositional ternary diagram comparing sandstones deposited in different rift segments of MRS. Data for units in Iowa (Red bed clastics) and Lake Superior region compiled from Anderson et al. (1987) and Ojakangas et al. (2002), respectively. ........ 64

# List of Tables

Table 3-1 : Samples for petrographic analysis, collected from different depths in NP#1, KS….. 17

Table 3-2 : Classification and symbols of grain types used in the provenance diagram (modified after Dickinson, 1985). ........................................................................................................ 20

Table 3-3 : Major provenance types and key compositional aspects of derivative sands (Dickinson,1985) ............................................................................................................ 21

Table 4-1 : Calculated averages and maxima of primary constituents for the quantified thin sections in different core sections. Modal grain size in mm, numerical sorting (dimensionless), and extrabasinal constituents in percentage (lithics include PRF- plutonic rock fragments, MRF- metamorphic rock fragments, VRF- volcanic rock fragments, SRF- sedimentary rock fragments)........................................................................................ 40

Table 4-2 : Calculated averages and maxima of diagenetic constituents for the quantified thin sections in different core sections. Modal grain size in mm, numerical sorting dimensionless, and diagenetic constituents in percentage. .................................................. 42

# Acknowledgements

I would like to thank Dr. Karin Goldberg for her guidance and all the efforts she put into me and this project. She has been more than a mentor to me, and this wouldn’t be possible without her. I would like to extend my gratitude to my committee members, Dr. Kempton and Dr. Adam, for their valuable insights.

This research has been financially supported by the Association for Women Geoscientist, Osage Chapter, for which I am grateful to them. Also, I would like to thank the Kansas Geological Survey for letting me borrow the cores from their core library in Lawrence, Kansas.

Lastly, I am indebted to my family and friends, new and old, for their continuous support and encouragement.

# Chapter 1 - Introduction

The Midcontinent rift system (MRS), otherwise known as the Keweenawan rift, is undoubtedly one of the most interesting structural features existing in North America. It has been interpreted as a failed triple-junction rift developed over a mantle plume (Ojakangas et al., 2001). This horseshoe-shaped 1.1 Ga-old thermo-tectonic structure stretches from south-central Kansas into Lake Superior and, from there, into Michigan and Ohio (Figure-1.1). The presence of the rift has been confirmed using gravity and magnetic data, which show a central gravimetric-magnetic high flanked by gravimetric-magnetic lows (Berendsen, 1997). The intensity of rifting and magmatism is highest beneath the Lake Superior zone, where up to 30 km of rift infill includes 20 km of basalt flows overlain by 10 km of post-volcanic clastic sedimentary rocks (Hinze et al., 1992).

Structural modeling of the data gathered from the Lake Superior region suggest a timeframe for rift activities that start as early as ca. 1.15 Ga, when regional volcanism initiated the rift, followed by the initial phase of rifting at about 1.12 Ga (Malone et al., 2016). The fault-controlled extensional basin was receiving flood basalts by 1.109 Ga, which finally gave way to post-rift volcanism and sedimentation in a subsiding basin by ca. 1.09 Ga (Malone et al., 2016). Contemporaneous development of the Grenville orogeny along the eastern margin of North America (ca. 1.3–0.98 Ga), which culminated in the assembly of Rodinia (Malone et al., 2016), potentially makes the history of the MRS a complicated one.

Despite the absence of outcrops in other regions (except Lake Superior, where the rift is exposed), gravity, magnetic and seismic data provide enough evidence to testify to the continuation of the rift to the south and to delimit it (Figure-1.1) (Elling et al., 2019). Subsurface data from boreholes have also been used to attest to the presence of rift successions in Michigan and Kansas

(Ojakangas et al., 2002; Berendsen, 1997). The Bouguer Gravity anomaly map of Kansas clearly shows the extension of the MRS (Figure-1.2) (Xia et al., 1996). The anomalies revealing the rift are interpreted as resulting from a basin filled with highly magnetic and dense volcanic rocks, which were later juxtaposed with less magnetic and dense rocks due to reverse faulting (Craddock et al., 1963; King and Zietz, 1971).

Along with the gravity and magnetic data, seismic profiling has been particularly useful for locating the extension of the rift in KS. The identification has been made by interpreting seismic data from the Consortium for Continental Reflection Profiling (COCORP) lines.

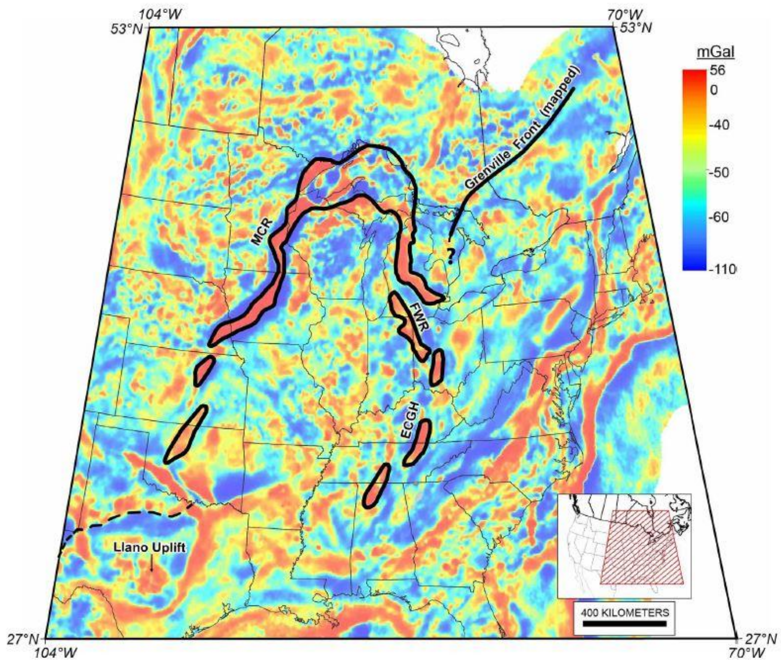


Figure 1.1 : Gravity anomaly map showing the regional extent of the MRS (Stein et al., 2018).

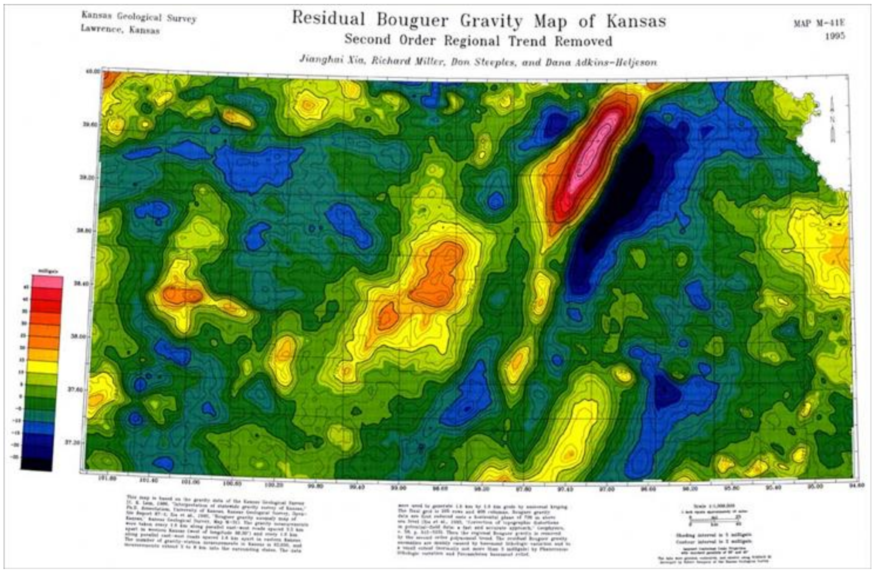


Figure 1.2 : Residual Bouger gravity map of Kansas, the second-order regional trend removed (after Xia et al., 1996).

Proprietary seismic reflection data collected by Texaco revealed that the Noel Poersch#1 well, the primary source of core data for this study, is located on the north-east margin of the MRS in KS (Berendsen, 1997).

Even though several geophysical studies have confirmed the presence of the MRS in Kansas (Halls, 1978; Serpa et al., 1984; Van Schmus and Hinze, 1985; Lam and Yarger, 1989), a lot is yet to be investigated regarding the evolution of the rift basin and its sedimentation pattern. For example, there are hardly any data available on the depositional processes and environments in response to rift evolution or the provenance of the rift fill. Hence, this research aims to study the rift sedimentation in Kansas at different rift-evolution stages. The research project focuses on characterizing the sedimentary rocks obtained from this well, describing the facies to interpret the depositional processes and environments, and analyzing the provenance of sediments in the rift succession to identify the change in source area related to rift evolution and to compare it to the units from other parts of the rift. It also attempts to propose a depositional model for the rift fills in KS.

# Chapter 2 - Geologic background

## 2.1 Identification of the rift and its structure in Kansas

The first steps towards the identification of the MRS in Kansas were taken in the early '40s, when a "long narrow belt of positive gravity anomaly", extending at least 1200 km southwestward from Lake Superior into Kansas, was identified and reported by Woollard (1943). Its definition moved forward when Thiel (1956) found a strong spatial correlation between this anomaly and the Keweenawan rocks from the Lake Superior area and proposed the name "Mid-continent gravity high".

However, the breakthrough in the identification and modeling of the rift was provided by Serpa et al. (1984). These authors analyzed seismic data from the Consortium for Continental Reflection Profiling (COCORP) lines across the northeastern part of Kansas, which revealed a very prominent central basin and related features of the MRS. The interpretation of the deep seismic profile indicated a 40 km wide, asymmetric rift basin plunging to the west, bounded by easterly dipping normal faults (Serpa et al., 1984). Later, Somanas et al. (1989) reprocessed some of the data and interpreted the presence of intrusive bodies on the seismic lines.

The gravity and magnetic data delineate the rift in the north-central part of Kansas (Figure-1.2). Rift development in Kansas is somewhat different from other parts of the MRS, such as the Lake Superior region, in the sense that this southern portion was less developed in terms of rift geometry, showing an asymmetrical half-graben due to the cessation of the rift (McSwiggen et al., 1987).

There has been ample evidence for the rift geometry from seismic studies by Serpa et al. (1984), which show the presence of low-angle, normal faulting contributing to the development of a rift basin in the southern segment of the MRS in Kansas. This, in association with an extensive crustal spreading of about 29 km (Serpa et al., 1984) during rifting, points to rift development as graben or half-grabens, rather than the previously proposed simple sag basin (Berendsen, 1997) (Figure-2.1).

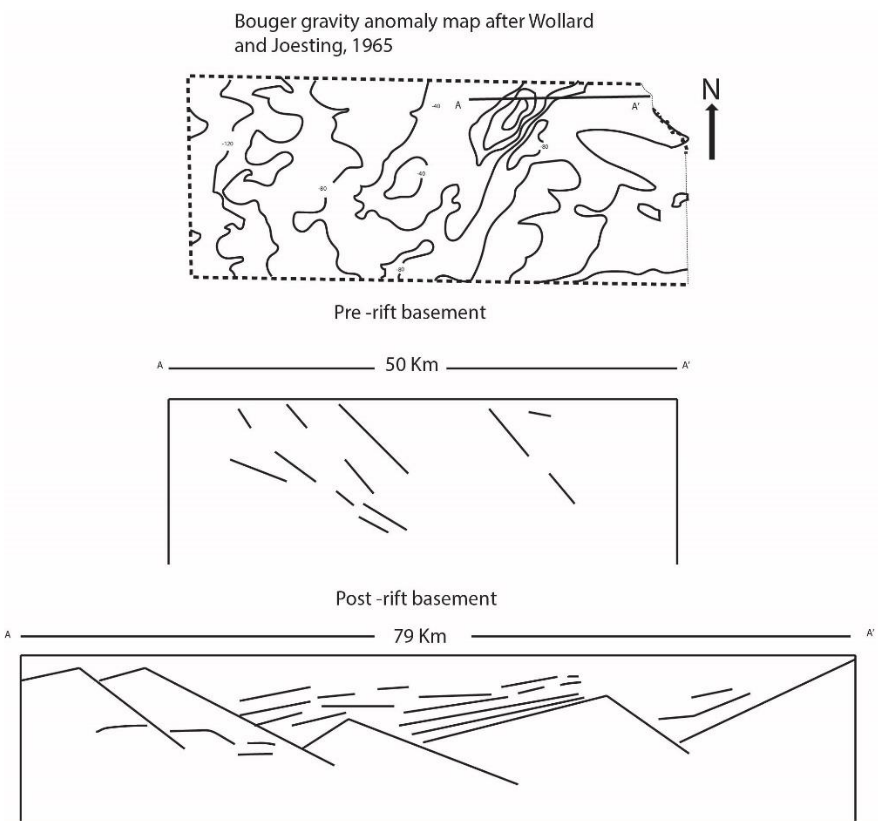


Figure 2.1 : Proposed model for the MRS basin structure and bounding faults in KS.

Analogous to Bosworth's (1987) model for the East African Gregory rift, McSwiggen (1987) proposed an arrested stage of rift development in Kansas. In his model, Bosworth (1986) explained the development of a half-graben, which initially started as a graben bounded by two faults, and the eventual truncation of one of the faults at greater depth locked the truncated fault, giving rise to a half-graben. Based on this model and the profile from Serpa et al. (1984), McSwiggen (1987) proposed that this southern terminus of the rift in Kansas might not have developed to the same extent as in the rest of the MRS. Additionally, this model also explains the thinner volcanic basin in Kansas compared to other parts of the rift, since the lesser degree of development could have barred the development of an extensive conduit system for extrusion of volcanic material (McSwiggen et al., 1987). However, different from Serpa (1984), Woelk and Hinze (1991) re-evaluated the basin as bounded by reverse rather than normal faults. The reverse faults have been attributed to a thrusting event that led to a compression east of the MRS, reactivating the normal faults and leading to reversal resulting from compression during the Grenville Orogenic event (Soofi & King, 2002).

The proposal that rift development in Kansas had a different evolutionary history that does not match other parts of the MRS is speculative, since there are no studies of the rift evolution through time, establishing the evolutionary stages integrated into a rift evolutionary model in KS. The integration of the geophysical and core data can be revolutionary in terms of providing a model that can explain changes in the development of the rift basin in Kansas compared to the rest of the rift system. A detailed facies and petrological study are vital to understand the sedimentary environments of accumulation in the rift as well as the source areas contributing to the rift basin in KS.

## 2.2 Sedimentology of the rift

Most authors suggest that the opening of the MRS was caused by a mantle plume centered on the Lake Superior area (Behrendt et al., 1990; Nicholson & Shirey, 1990; Paces & Bell, 1989). This plume was responsible for the uplift of the lithosphere, which created a broad dome centered on Lake Superior that was eventually breached by the MRS (Hinze et al., 1992). The presence of the plume, in that area, caused the radial drainage pattern, topographic dome, and regional gravity anomaly, as proposed by Hinze (1992). The thermal anomaly associated with the plume, therefore, controlled the elevation, which in turn influenced the erosional level in the source area and subsidence rates in the rift basin. These factors, in association with the rift structure, controlled sedimentation within the rift basin.

Most rift basins are thought to be structurally composed of asymmetrical half-grabens in local scale (Bosworth et al., 1986). In order to understand the associated sedimentation, it is important to describe the architecture of the rift basin, as it is strongly influenced by the displacement geometry of the bounding fault system (Withjack et al., 2002). The fault and fault-related topography controls the sedimentary systems within the rift basin by controlling accommodation (Barr, 1987; Leeder and Gawthorpe, 1987), i.e., the space available for potential sediment accumulation (Jervey, 1988). Also, the structures within the rift basins affect the depositional pattern by causing uplift and erosion, which in turn control accommodation, and sediment transportation and deposition (Withjack et al., 2002). Thus, the basin fill can be classified in accordance with the different stages of its tectono-stratigraphic evolution.

Bosence (1998) proposed a classification categorizing the stratigraphic units of rift basins into pre-rift, syn-rift, and post-rift successions, separated by two unconformities, namely syn-rift and post-rift unconformities. According to this model, the onset of rifting triggers a complex fault-related topography that guides sediment accumulation and controls the erosional and sedimentological process. This phase can be dominated by igneous rocks, and the sediments deposited during this phase are mostly controlled by the rift basin architecture (Berendsen, 1997). At this stage, the extended crust undergoes regional subsidence, the footwall crests are uplifted and erode, becoming the source of the sediments. As the rifting advances, a complex drainage basin and the changing relationship with the structures control the thickness of the syn-rift strata (Bosence, 1998).

An unconformity separates the syn-rift units from the overlying post-rift units. Usually, these unconformities develop around the rift shoulders and provide information about thermal subsidence. The rift shoulders become progressively buried by post-rift basin fill, in response to slow subsidence of the rift basin (Bosence, 1998). Subsidence in this stage is controlled by cooling and an increase in the density of the lithosphere and asthenosphere, augmented by sediments and water loading (Bott, 1992). The post-rift strata are characterized by thick onlap and offlap, with surfaces dipping into the enlarging accommodation in the basin center (Bosence, 1998), as the basin slowly evolves into either a passive oceanic basin margin or, in this case, a failed rift.

Since most of the outcrops of the MRS are found in the Lake Superior region, this area has been extensively studied for the sedimentary fill of the rift basin (Ojakangas and Dickas, 2002). Four different assemblages related to the rift in that area have been suggested by Ojakangas et al. (2001) (Figure-2.2). In general, the rift succession in the north includes syn-rift and post-rift succession overlying the Precambrian rocks. The syn-rift succession comprises of lava flows (loosely termed “Portage Lake Lava Formation”), interbedded with a 30-meter-thick succession of sedimentary rocks (known as the “interflow sequence”) deposited during volcanic quiescence (Merk and Jirsa, 1982). The latter makes up about 3% of the syn-rift rock volume (Berendsen, 1997).

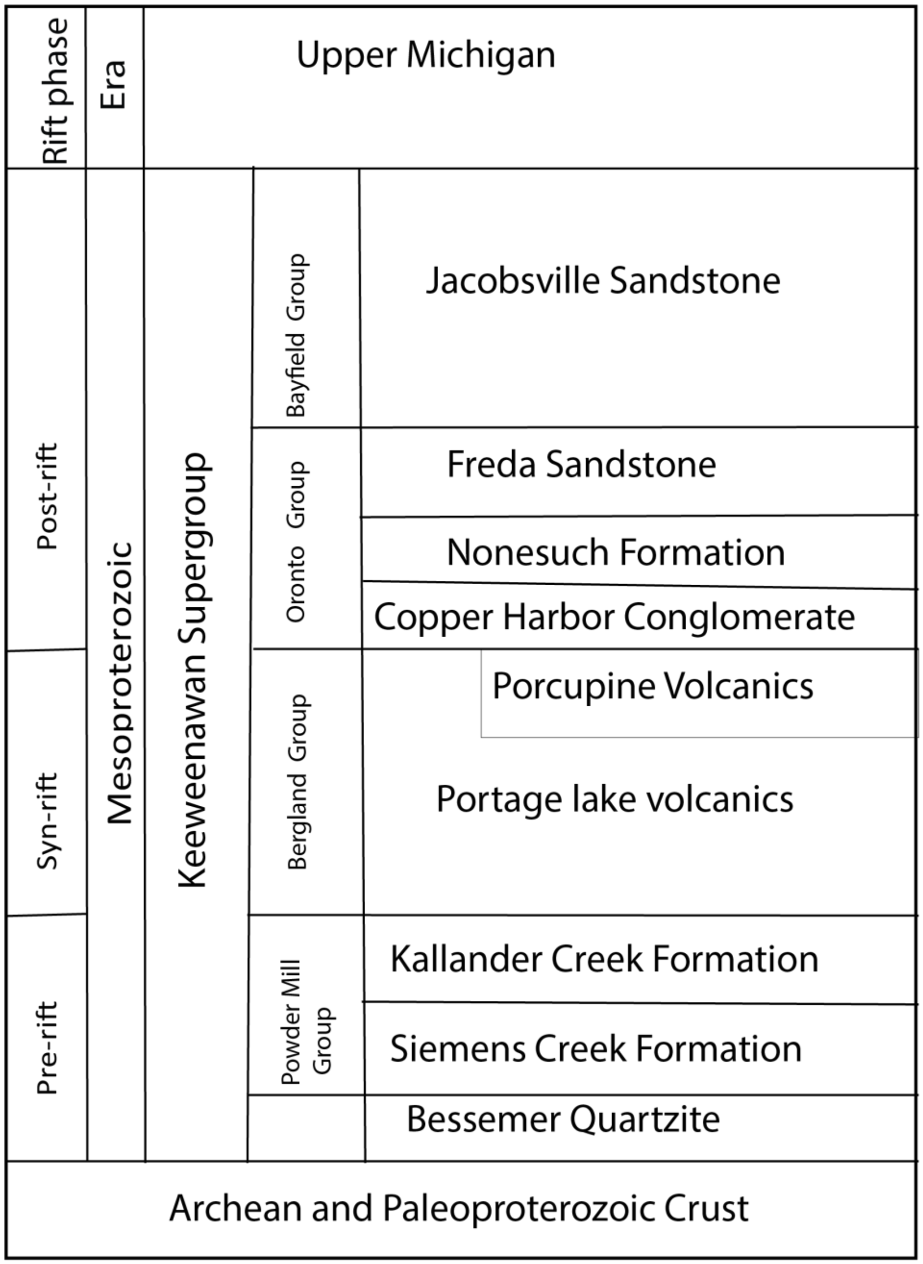


Figure 2.2 : Lithostratigraphic column of MRS basin fill from Upper Michigan (modified from Ojakangas and Dickas, 2002).

A thick post-rift unit of about 10 km in the Lake Superior region (Stein et al., 2018) overlies the syn-rift unit, which, in outcrop, includes the Oronto Group and the Bayfield Group. Both of these stratigraphic units are composed of red bed, alluvial fan - fluvial successions.

In contrast to the data available for the rift succession in Lake Superior, the sedimentary fill of the rift in Kansas is yet to be studied in detail, especially pertaining to rock data. The sedimentary package of the rift in Kansas has been loosely called the Rice Formation (Berendsen, 1997).

This unit occurs at the top of the Precambrian basement in two rather extensive areas in Kansas, referred to as the "Western Basin" (or the Rice Basin) and the "Eastern Basin" (Berendsen, 1997). The former one extends from Reno County to Washington County, and the latter one runs parallel to this one to the east (Berendsen, 1997). The western and eastern basins are separated by a north-northeast trending unit of mafic igneous rocks that follow the axis of the midcontinent geophysical anomaly (Scott, 1966).

The Rice Formation is composed of reddish-brown, fine-grained feldspathic sandstone, commonly conglomeratic (Berendsen, 1997). Scott (1966) suggested a marine or lacustrine depositional environment for this formation, as it contains limestone and dolomite interbedded with sandstone and shale.

The Noel Poersch#1 well, drilled in the eastern flank of the geophysical anomaly (Figure-2.3), provides valuable insights into the rift infilling. Located in Washington County, it was drilled back in 1984 as a wildcat well. It is the deepest well ever drilled in Kansas, with a total depth of 11,300 feet (3444 m). The top of the Precambrian is at a depth of 2,846 ft (867 m). The rift succession can be broadly categorized into two successions: the lower succession (7,429-11,300 ft; 2,264-3,444 m) is dominated by clastic sediments, while the upper one (2,846-7,429 ft; 867-2,264 m) is composed mostly of mafic volcanic rocks (Berendsen, 1997) (Figure-2.4).

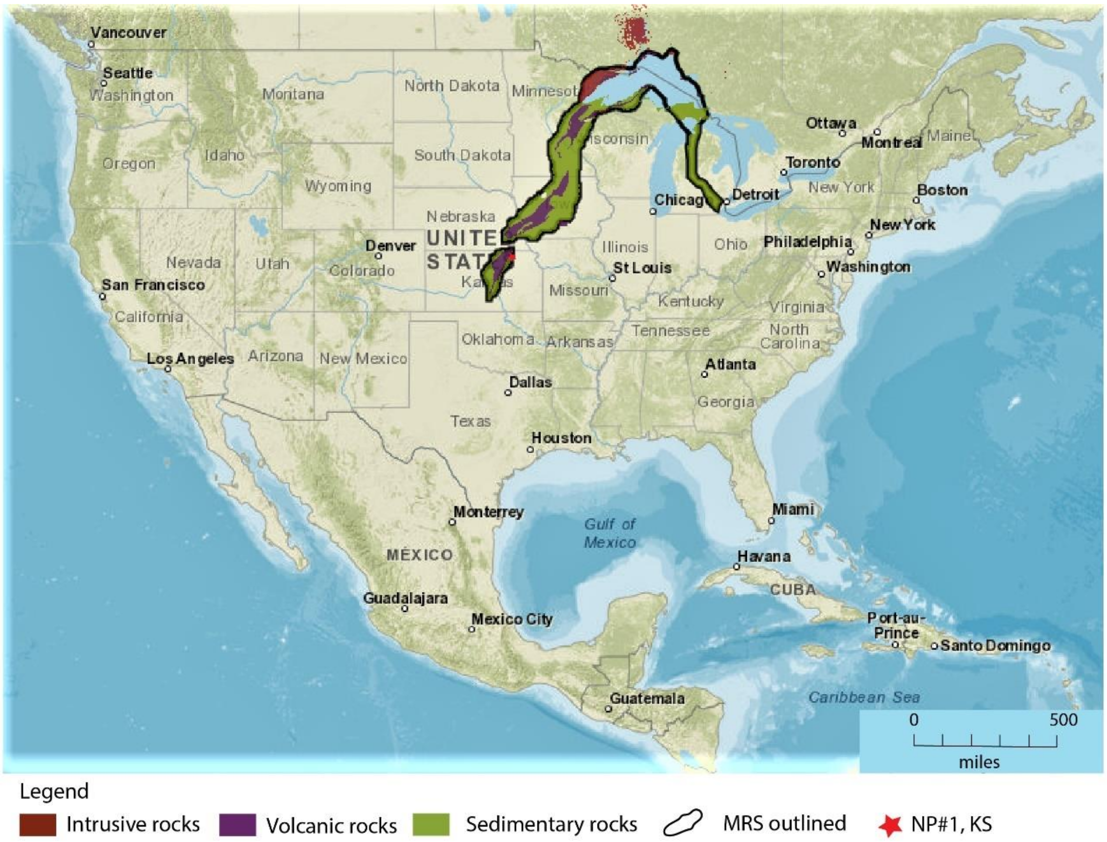


Figure 2.3 : Location map of the Midcontinent Rift System showing the rift segment in KS with the approximate location of the Noel Poersch (NP#1). Extracted from "Mineral deposits of the Midcontinent Rift System" https://www.arcgis.com/apps/MapSeries/index.html?appid=6687aedec0c2452db15b85ea253fb842).

Three distinguishable periods of igneous activity appear within the lower sedimentary-dominated succession, while the upper volcanic-dominated succession includes at least five thin interflow sequences. The existence of these two successions indicates a radical change in tectonic settings and depositional conditions that took place at depths around 7429 feet (2264 m).

In the preliminary report produced by Kansas Geological Survey, well cuttings were analyzed and the rock succession has been suggested to comprise syn-rift deposits (Berendsen, 1997), based on the correlation with COCORP seismic profile and the textural and compositional immaturity of the deposits. The report proposed the hinterland rift shoulder as the source for the deposit and concluded that the rift segment in KS is younger in comparison with other segments of MRS to the north, with limited volcanism. Also, a much younger age was obtained on the volcanics in NP#1 compared to other rift segments of MRS which confirmed McSwiggen's (1987) proposal of a less-developed rift in Kansas.

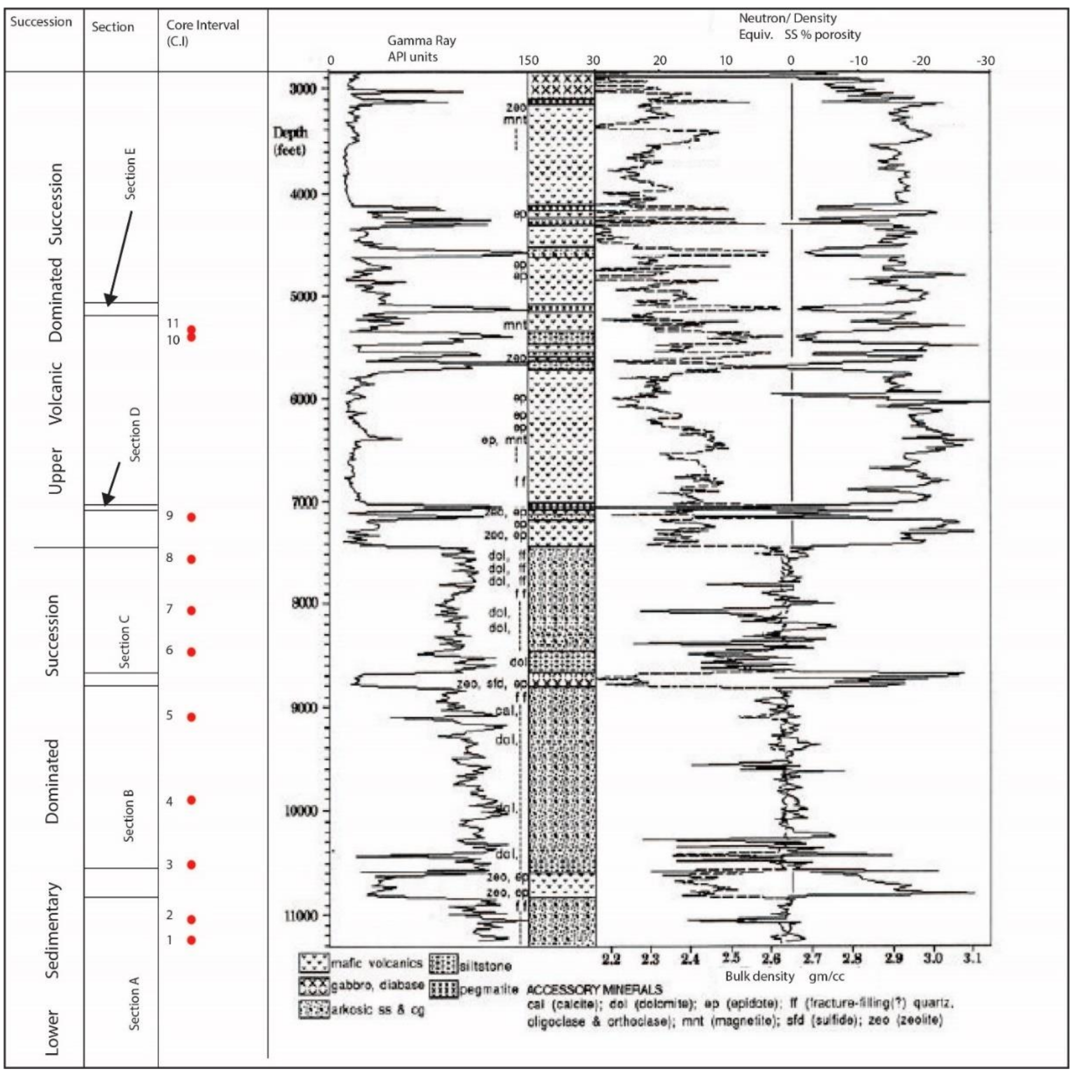


Figure 2.4 : Wireline log of Noel Poersch#1, KS, showing the eleven core intervals used in this study (modified from Berendsen, 1997).

# Chapter 3 - Methods of investigation

The purpose of this research was to study the sedimentary fill of the Midcontinent Rift System in Kansas and establish the depositional environments for the rift succession to understand their association with rift-basin architecture and hence rift evolution. For that, the approach was to identify the facies and sedimentary provenance through facies and quantitative petrographic analyses.

## 3.1 Core description and facies analysis

The only well in KS that reaches the MRS is Texaco Noel Poersch#1 (Figure 1.1). This well, with a total depth of 11300 ft, has continuous wireline logs but only a few cored intervals. Access to the cores was provided by the Kansas Geological Survey. Prior studies identified two successions (Berendsen, 1997): the upper one (up to depths of 7,429 ft) is composed of dominantly volcanic rocks, with sparse sedimentary interbeds, whereas the lower succession (at depths of 7429-11300 ft) is dominated by sedimentary rocks, and thus was the focus of this study (Figure-2.4).

The studied depth range, from 5395 ft (1644 m) to 11296 ft (3443 m), was comprised of a total of 71.3 ft (21 m) of cores, i.e. nearly 99% of the sedimentary sequence is missing, which was a limitation for this study. The wireline log data of the Noel Poersch#1 suggest two periods of igneous activities within the lower sedimentary-dominated succession (Figure-2.4) at depths of 10840-10622 ft and 8810-8676 ft. These volcanic intervals were used to divide the lower, sedimentary-dominated succession into three distinct sections, namely sections A, B and C. On the other hand, the upper, volcanic-dominated succession has some thin interflow sedimentary units (Berendsen, 1997) that reflect periods of quiescence. Three cores retrieved from those depths were studied for this research and were categorized as section D and section E (Figure-2.4). Eleven core intervals (C.I) were studied in total for this research (Figure-2.4)

Detailed description (Scale=1:30.5) of these cores to gather sedimentological data for facies identification included texture, composition, sedimentary structures, and diagenetic features. They are displayed as a composite sedimentological log (Appendix-A). The concept of facies used in this project is Reading's (1996), in which facies are defined by lithological attributes such as color, grain size, roundness, sorting, grain composition, and sedimentary structures.

The facies classification scheme used here was adapted from that proposed by Miall (1985) for fluvial systems, in which grain size and sedimentary structures are represented by letters. The first letter is capitalized and represents grain size (i.e. G for gravel, S for sand, F for fine-grained sediments). Letters that follow are in lower case and indicate texture and/or sedimentary structures (e.g., t for trough cross-stratification). The identified facies were then organized in a lithofacies table, with illustrative plates for each lithofacies, and grouped into facies associations, which corresponded to a group of facies genetically related to one another, representing sub-environments of deposition within a depositional system (Collinson, 1996; James and Dalrymple, 2010).

The stratigraphic analysis through the construction of lithological logs has the advantage of summarizing a large volume of data and providing an immediate view of the vertical facies succession (McCoy et al., 2010). The lithological logs were constructed with grain size in the x-axis and bed thickness in the y-axis, complemented by sedimentary structures, facies code, facies description (grain size, color, texture, and any other significant attributes), photographs and collected samples. Lithological logs were later digitized with Adobe Illustrator® and hence standardized for presentation, with a header that includes a key to the symbols and facies codes (Appendix-A).

## 3.2 Quantitative petrographic analysis

Twenty-seven samples were selected for quantitative petrographic analysis (Table-3.1). Sample selection was guided by facies variations, where at least one sample was selected for each of the identified facies. These samples were made into thin sections and were subjected to further investigation using a conventional polarizing optical microscope with an attached high-resolution camera. Thin sections were stained with a dilute hydrochloric solution of alizarin red-S and potassium ferricyanide to differentiate between calcite and dolomite (cf. Dickson, 1965) by applying 1-2 drops of the solution to the entire thin section, letting it react for a few seconds and rinsing with water. Different carbonates stain differently; for example, non-ferroan calcite stains pink while ferroan calcite turns into purple, as opposed to dolomite, which does not change colors.

Systematic quantitative petrography of thin sections impregnated with blue dye to identify pores was carried out to determine primary and diagenetic constituents, as well as to refine facies description. Petrographic information was stored and processed in Petroledge® (De Ros et al., 2007). The descriptive information noted for each thin section includes identification, microscopic textural (structures, grain size range, modal grain size, sorting, sphericity, roundness, orientation, packing, etc.) and compositional features. Grain size was measured using the built-in microscopic scale (in mm/micron), and averages were assigned to grain size based on the Wentworth Scale (Udden, 1914; Wentworth, 1922). A dimensionless value was assigned for sorting, identified by using the built-in visual aid in Petroledge® where values range from very well sorted samples (<0.35),well-sorted (0.35-0.50) moderately sorted (0.50-0.70), poorly sorted (0.70-2) to very poorly sorted (>2) ones.

The volume of detrital and diagenetic components was determined by counting 300 points in each of the thin sections utilizing the Petroledge® Compositional Quantification Module, where description and quantification of all the detrital, diagenetic, and pore type constituents, along with the habits, locations, paragenetic relations and any modifiers, were recorded. After carrying out the detailed compositional and textural analysis in thin section, these data were processed with the help of the Interpretation module, which provided an automatic interpretation, including compositional, textural, and provenance classifications.

Table 3-1 : Samples for petrographic analysis, collected from different depths in NP#1, KS.

| Sections | Core intervals (C. I) | Sample ID | Representative Facies Code |
|---|---|---|---|
| E | 11 | NP1-5396 | Ff |
| | 10 | NP1-5404.2 | Fl |
| | | NP1-5406 | Gcm |
| D | 9 | NP1-7152 | Gcm |
| | | NP1-7153 | Fd |
| | | NP1-7154 | Sm |
| | | NP1-7154.2 | Gci |
| C | 8 | NP1-7568 | Sh |
| | 7 | NP1-8053.2 | She |
| | | NP1-8056.6 | She |
| | 6 | NP1-8480 | Fm |
| B | 5 | NP1-9164.7 | She |
| | | NP1-9170 | Sle |
| | 4 | NP1-9951 | Spe |
| | | NP1-9954 | Sp |
| | | NP1-9957 | Sp |
| | | NP1-9962 | Sp |
| | 3 | NP1-10509 | Sc |
| | | NP1-10510 | Sc |
| | | NP1-10512 | She |
| | | NP1-10515 | Sc |
| A | 2 | NP1-11061 | Sm |
| | | NP1-11063.5 | Sm |
| | 1 | NP1-11290 | Sle |
| | | NP1-11293.8 | Sle |
| | | NP1-11295 | Sh |
| | | NP1-11296 | Sle |

| Key for facies code |
|---|
| Gcm - Clast-supported conglomerate |
| Gci - Intraformational conglomerate |
| Sh - Sandstone with horizontal lamination |
| Sh(e) - Sandstone with horizontal lamination and inverse grading |
| Sl - Sandstone with low-angle cross stratification |
| Sl(e) - Sandstone with low-angle cross stratification and inverse grading |
| Sm - Massive sandstone |
| Sp - Cross-stratified sandstone |
| Sp(e) - Cross-stratified sandstone with inverse grading |
| Sr - Sandstone with ripple cross lamination |
| Sw - Sandstone with symmetrical ripples |
| Sc - Sandstone with crinkly lamination |
| Ff - Sandstone with fenestral lamination |
| Fl - Laminated mudstone |
| Fm - Massive mudstone |
| Fd - Mudstone with soft-sediment deformation structures |

The compositional classification scheme used for this study follows McBride's (1963) (Figure-3.1), while the textural classification follows Folk's (1951), based on the proportions between gravel, mud, and sand content.

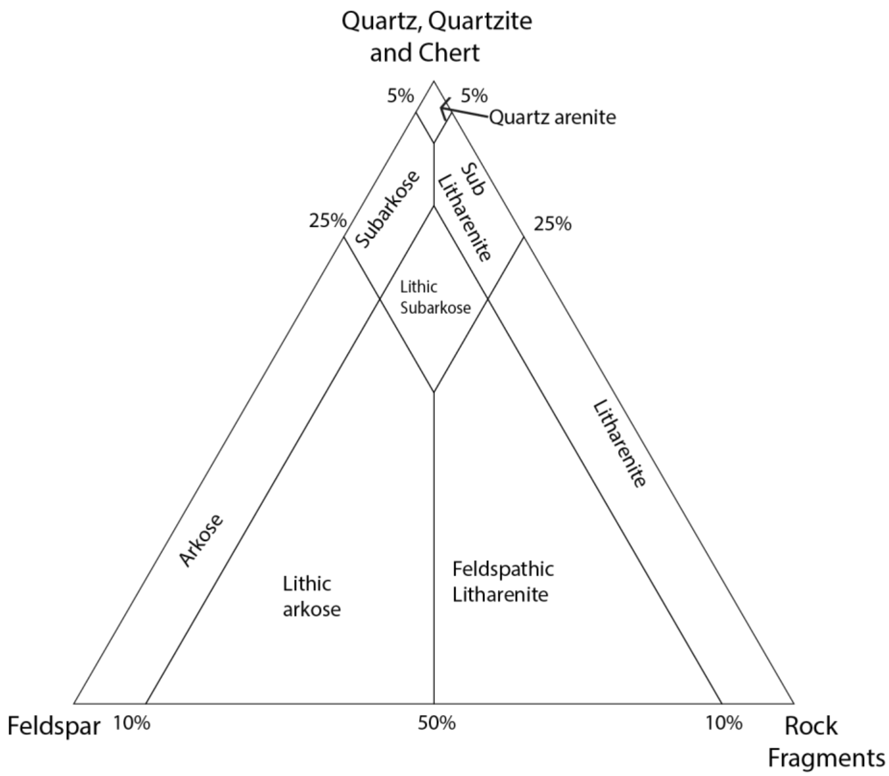


Figure 3.1 : Sandstone classification after McBride (1963)

Provenance analysis followed the Gazzi-Dickinson quantification method (cf. Zuffa, 1985). Based on the extrabasinal contribution to sandstone composition calculated from each thin section and plotted on a ternary diagram (Figure-3.2), provenance related to different tectonic compartments was assigned. This method assumes that provenance exerts a primary control on sandstone composition and, therefore, the sources for the detrital grains in a sandstone sample (Table-3.2) can be used to trace where the sediments derived from (Table-3.3). In this scheme, sand-sized crystals or grains within larger fragments (larger than 0.0625 mm) are assigned to the category of the crystal or grain, rather than to the category of the larger fragment. This successfully eliminates the compositional grain-size dependency related to the breakage of fragments into constituent grains (Ingersoll et al., 1984).

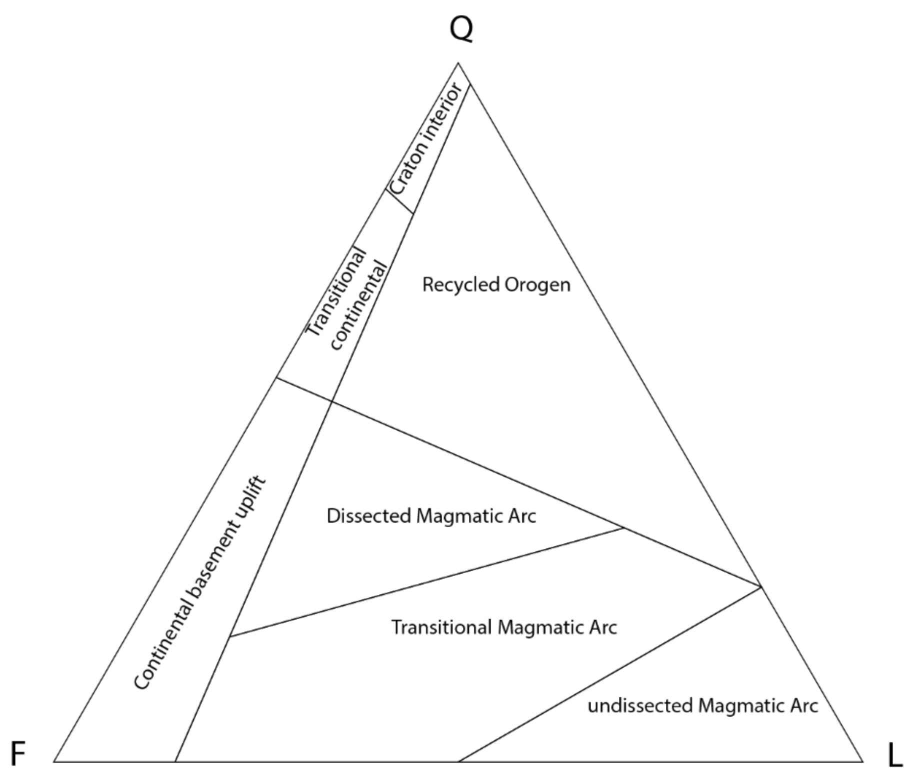


Figure 3.2 : Ternary plots of sandstone composition for provenance analysis (after Dickinson, 1985); refer to Table-3.2 for key.

Table 3-2 : Classification and symbols of grain types used in the provenance diagram (modified after Dickinson, 1985).

A. Quartzose Grains (Q=Qm+Qp)

Q=total quartzose grains
Qm= monocrystalline quartz (>0.625 mm)
Qp= polycrystalline quartz (or chalcedony)

B. Feldspar grains (F=P+K)

F=total feldspar grain
P= Plagioclase grains
K= K-feldspar grains

C. Unstable Lithic Fragments (L=Lv+Ls)

L= total unstable lithic fragments
Lv= volcanic/metavolcanic lithic fragments
Ls= sedimentary/metasedimentary lithic fragments

D. Total Lithic Fragments (Lt=L+Qp)
Lc= extrabasinal detrital limeclasts
(not included in L or Lt)

Diagenetic constituents replacing framework grains were used to reconstruct the original composition, and hence obtain a better estimate of the source area.

Table 3-3 : Major provenance types and key compositional aspects of derivative sands (Dickinson,1985)

| Provenance Type | Tectonic Settings | Derivative sand composition |
|---|---|---|
| Stable Craton | Continental interior or passive platform | Quartzose sands (Qt-rich) with high Qm/Qp and K/P ratios |
| Basement uplift | Rift shoulder or transform rupture | Quartzofeldspathic (Qm-F) sands low in Lt with Qm/f and K/P ratios similar to bedrock |
| Magmatic arc | Island arc or continental arc | Feldspatholithic (F-L) volcaniclastic sands with high P/K and Lv/Ls ratios grading to quartzofeldspathic (Qm-F) btholith-derived sands |
| Recycled orogen | Subduction complex or fold-thrust belt | Quartzolithic (Qt-Lt) sands low in F and Lv with Variable Qm/Qp and Qp/Ls ratios |

# Chapter 4 - Results and interpretations

## 4.1 Facies analysis

### 4.1.1 Core description and facies identification

Sixteen lithofacies, summarized in Figure 4.1, were identified in the studied cores (Figure-4.2). Figure-4.3 displays representative photographs (and, in some cases, photomicrographs) of the facies. The facies codes are displayed in the composite sedimentary log in Appendix-A.

| Facies Code | Description | Interpretation | |
|---|---|---|---|
| Gcm | Reddish brown, clast-supported massive conglomerate; very poorly to poorly-sorted, with subangular- subrounded pebbles and granules (up to 5.2 cm) rich in plutonic and volcanic rock fragments, with some mud intraclasts, very little (<5%), medium sand matrix; locally with irregular mud drapes and/or discontinuous mud intrusions along fracture planes. | Bedload deposited in subaqueous environments by strong currents, with erosion and incorporation of adjacent muddy sediments into extrabasinal load; high depositional energy. | |
| Gci | Reddish brown, clast-supported massive intraformational conglomerate; poorly-sorted, with subangular granule-sized (up to 1.2 cm) mud intraclasts mixed with coarse to very coarse sand grains , 5-7% of matrix of fine sand; locally discontinuous milimetric mud films. | Reworking of semi-consolidated muddy sediments in subaqueous environments by strong currents; high depositional energy. | |
| Sh | Reddish brown to gray, coarse to fine sandstone with horizontal, grain-size and/or compositional (mafic/felsic) lamination; poorly-sorted, subrounded-subangular grains; carbonate cementation preferentially along coarser laminae | Deposition of plane beds in subaqueous environments by currents under upper flow regime. | |
| Sh(e) | Reddish brown to gray, very fine to fine sandstone with horizontal, pinstripe and inversely-graded lamination; moderately-sorted, subrounded-subangular grains | Deposition of plane beds by wind under upper flow regime. | |
| Sl | Reddish brown, fine sandstone with low-angle cross stratification; moderately- to poorly-sorted. | Deposition of washed-out and/or humpback dunes in subaqueous environments under transitional between critical and supercritical flows. | |
| Sl(e) | Reddish brown, very fine to fine sandstone with low-angle cross stratification, pinstripe and inversely-graded lamination; moderately-sorted, rounded grains. | Deposition of washed-out and/or humpback dunes by wind under transitional between critical and supercritical flows. | |
| Sm | Grayish to reddish brown, coarse to very fine massive sandstone, locally with scattered granules and pebbles; poorly-sorted, locally with faint lamination and inclined millimetric carbonate veins. | Deposition of sediment gravity flows and/or de-stratification due to fluidization by dewatering. | |
| Sp | Reddish brown to gray, very fine to medium sandstone with planar cross stratification; moderately- to poorly-sorted, with subangular to subrounded grains; centimetric to millimetric laminae of medium to coarse sandstone with carbonate cementation. | Migration of straight-crested dunes in subaqueous environments by currents under lower flow regime. | |
| Sp(e) | Reddish brown to gray, fine sandstone with planar cross stratification, pinstripe and inverse-graded lamination; moderately sorted, well-rounded grains. | Migration of eolian, straight-crested dunes under lower flow regime. | |
| Sr | Reddish brown, fine sandstone with ripple cross lamination and asymmetrical ripples. | Subaqueous ripple migration by currents under lower flow regime. | |
| Sw | Reddish brown, fine sandstone, with symmetric ripples to supercritical ripple cross lamination; moderately-sorted; continuous mud laminae draping the ripples. | Subaqueous ripple migration under oscillatory flow regime. | |
| Sc | Reddish brown, fine sandstone with crinkly lamination composed of irregular, discontinuous mud laminae; with carbonate cementation spots. | Binding and trapping of sediment particles onto benthic microbial mat surfaces. | |
| Ff | Reddish brown mudstone with horizontally-elongated irregular-shaped fenestrae, commonly with flat bases and irregular tops, filled by cement. | Successive episodes of accretion and desiccation of microbial mats. | |
| Fl | Reddish brown mudstone with plane-parallel lamination and with discontinuous silt lenses. | Suspension settling from dominantly standing water. | |
| Fm | Reddish brown, massive mudstone, locally with millimetric faint lamination marked by very fine sand laminae; hematite staining. | Suspension settling from standing water; low depositional energy. | |
| Fd | Reddish brown mudstone with convolute lamination, irregular silt streaks, discontinuous millimetric clay laminae and faint climbing ripples. | Suspension settling from dominantly standing water, with plastic deformation of semi-consolidated sediments due to re-sedimentation and/or fluidization. | |

Figure 4.1 : Facies table with description and interpretation of the sixteen facies identified on the studied cores.

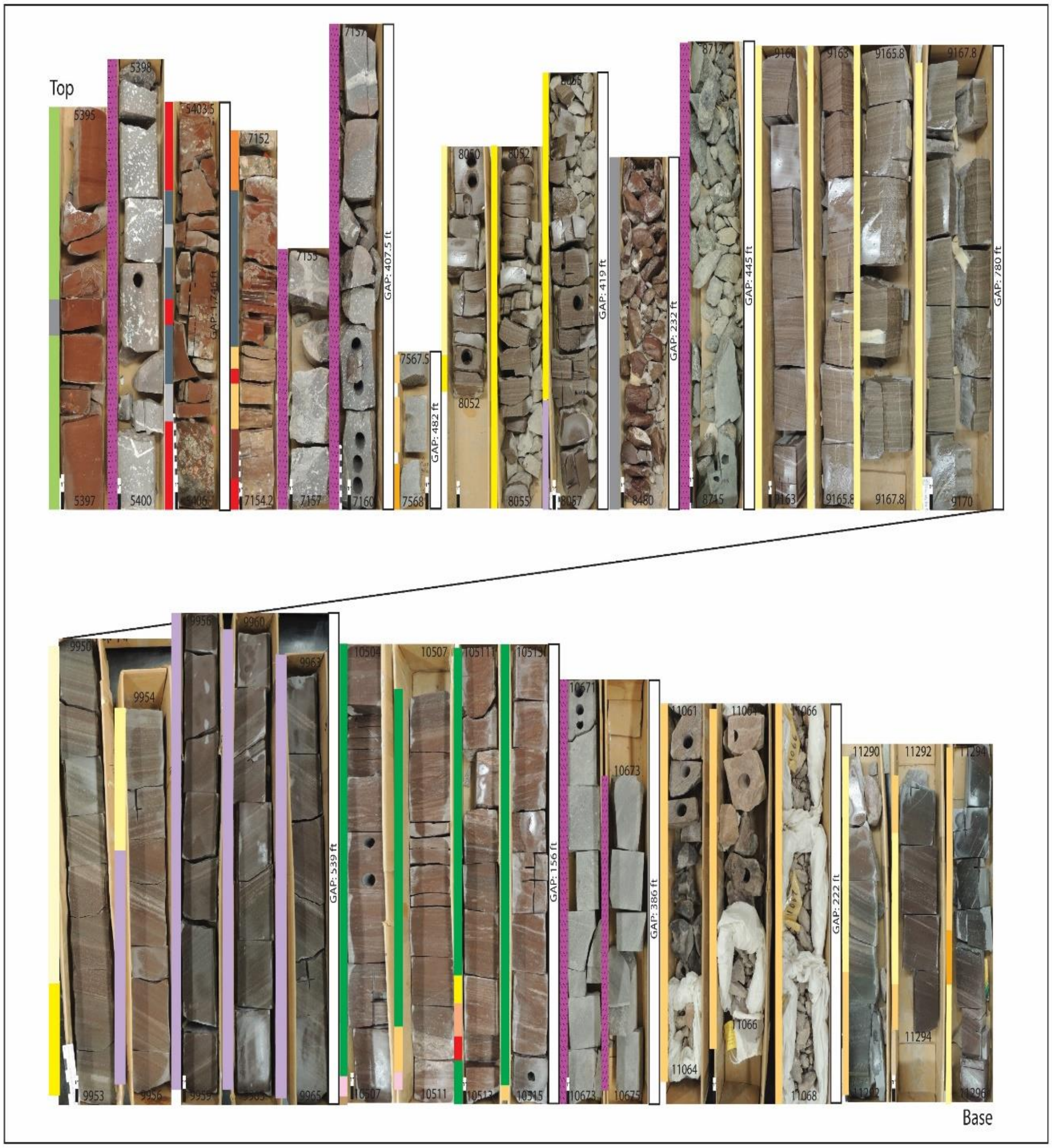


Figure 4.2 : Distribution of the identified lithofacies in the cores from NP#1. The colors in the bars adjacent to the core photographs correspond to the facies in Figure 4.1 (except for magenta, representing volcanic rocks).

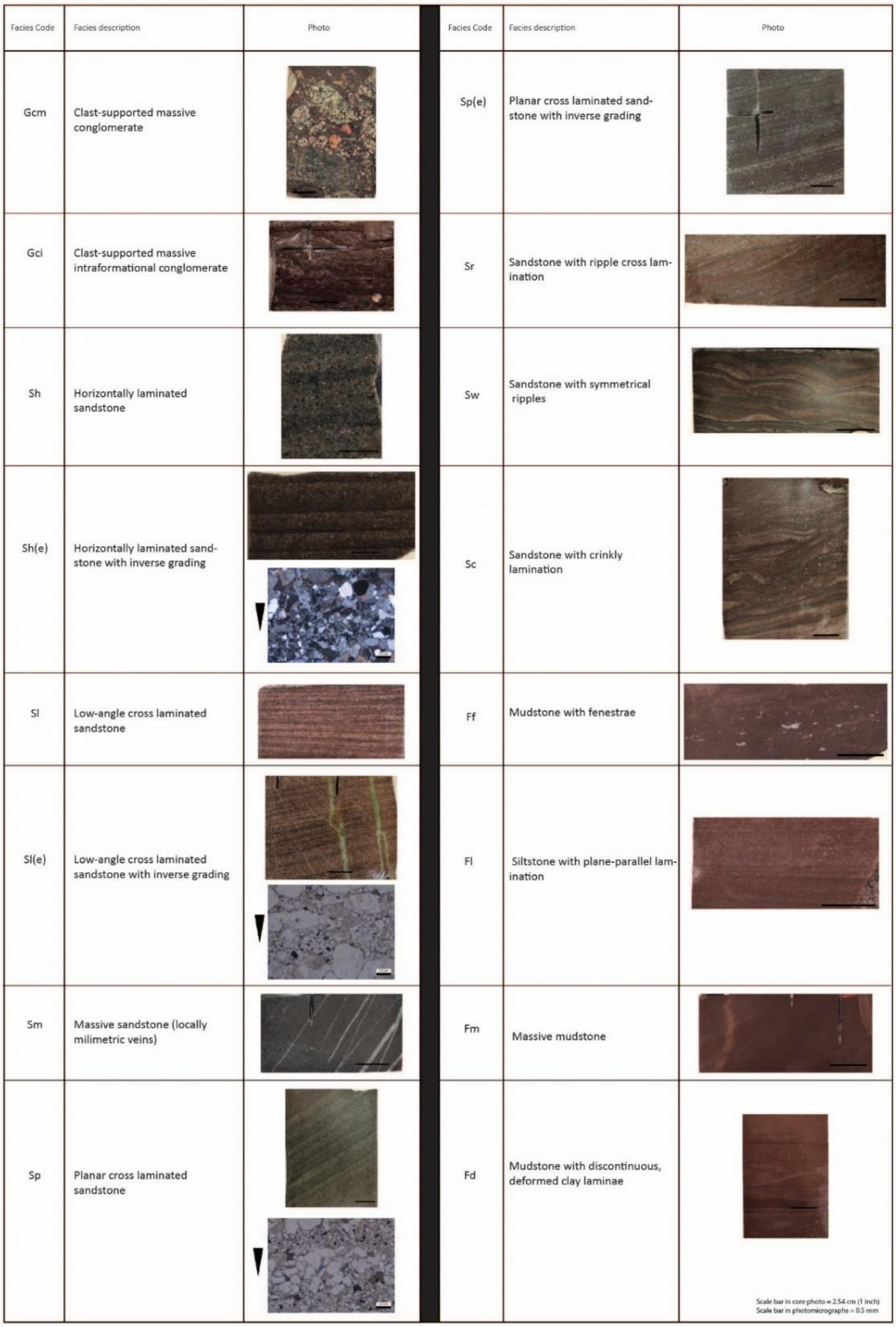


Figure 4.3 : Representative photos of the facies identified in the studied cores.

Figure-4.4 shows the distribution and abundance of the identified facies within the 66.16 feet of studied cores from NP#1.The identified facies fall into three broad categories, based on the modal grain sizes, i.e., gravel (>2 mm), sand (0.125-2 mm), and fine-grained (<0.125 mm), which (from gravel to fine-grained) reflect decreasing energy levels in the depositional environment.

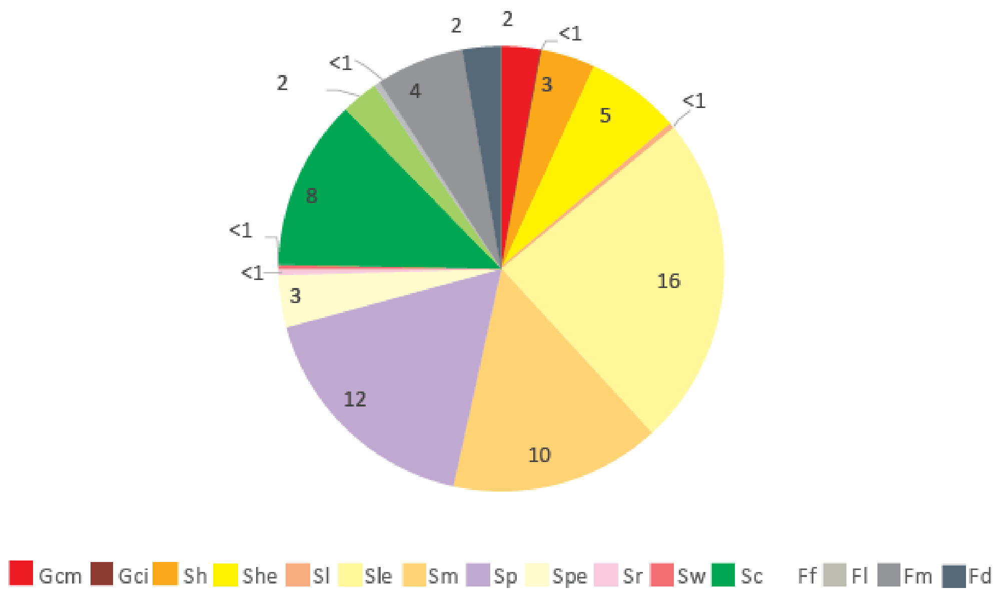


Figure 4.4 : Overall abundance (calculated as percentage over total thickness) of the identified facies in cores from NP#1.

The pie diagram (Figure-4.4) indicates that sandstone facies (S) are the most abundant in the analyzed cores, compared to minor mudstones (F) and conglomerates (G). The most abundant facies is Sle, followed by Sp, Sm and Sc, and together they comprise 70% of the total core. However, their distribution is not homogeneous amongst the different sections.

Section A, the lowermost section, includes only three facies, mostly Sm and Sle interbedded with minor Sh (Figure-4.5 A). Overlying this section, Section B contains numerous facies, of which the most abundant is Sle, followed by Sp and Sc facies, with thin interbeds of Sr and Sw (Figure-4.5 B). Subordinately, Spe and Sh are interbedded with very thin beds of She, Sm, Sl. In Section C, facies Fm is the most abundant, comprising the entire C.I 6. She and Sle are present with minor interbeds Sp, Sh and Sm (Figure-4.5 C).

The upper volcanic-dominated succession includes two sections, D and E. Both contain gravel, sand and fine-grained facies. Cores from Section D, consisting of Gcm, Gci, Sm and Fd, with Gcm being the most abundant facies (Figure-4.5 D). Section E is dominated by fine-grained facies, with Fl, Fd, Ff and Fm comprising 70% of the total thickness, with minor Gcm facies (Figure-4.5 E).

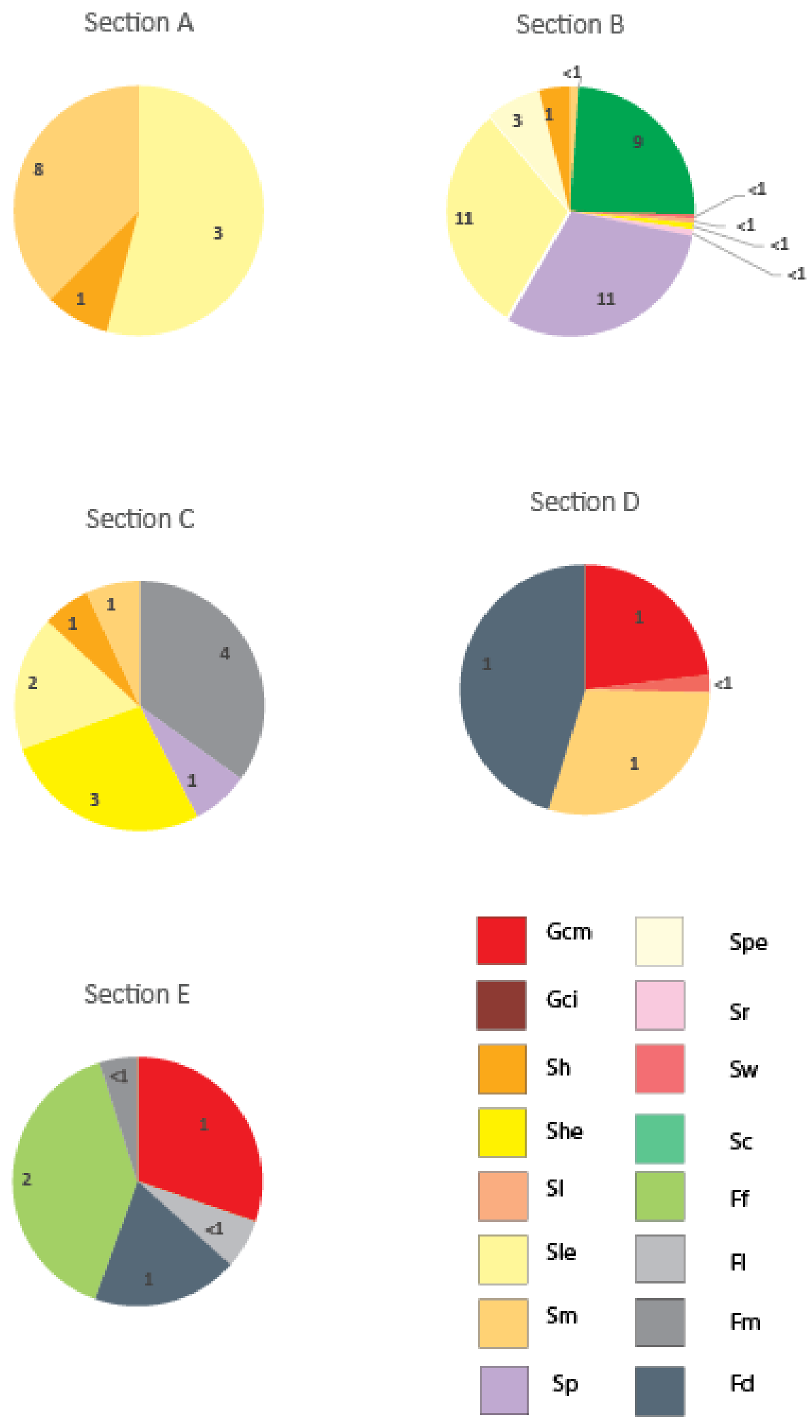


Figure 4.5 : Facies distribution within different sections for cores from NP#1.

### 4.1.2 Facies associations and depositional environments

The lithofacies identified from the cores were grouped into six facies associations: eolian, fluvial, lacustrine, mudflat/lake margin, alluvial fan, and fan delta facies associations. The description and interpretation of each facies association are displayed in Figure-4.6. Figure-4.7 displays the distribution of facies associations and vertical facies successions in the sedimentary log.

#### 4.1.2.1 Eolian Facies Association

The Eolian facies association comprises of successions up 15 feet thick, composed of moderately to well sorted sandstones, mostly low-angle cross stratification and inverse grading (Sle) interbedded with horizontal lamination and planar cross lamination, both with inverse grading (She and Spe, respectively) (Figure-4.6). It is found only within the lower sedimentary-dominated succession (Figure-4.7).

The interpretation as eolian deposits is based on the presence of pinstripe lamination and inverse grading, reddish-brown color, and well-sorted nature of the sand bodies (Nichols, 2009). The alternations of Sle and She marks the fluctuation of wind velocities, between transitional and upper flow regime. The interbedding between these facies is typical of sand sheet deposits adjacent to dune fields. The latter is characterized by successions of low to moderately dipping ($0-20^0$) cross-stratified sandstones (Boggs, 2014). Packages of Spe interbedded with Sle are suggestive of dune and dry interdune deposits (Boggs, 2014).

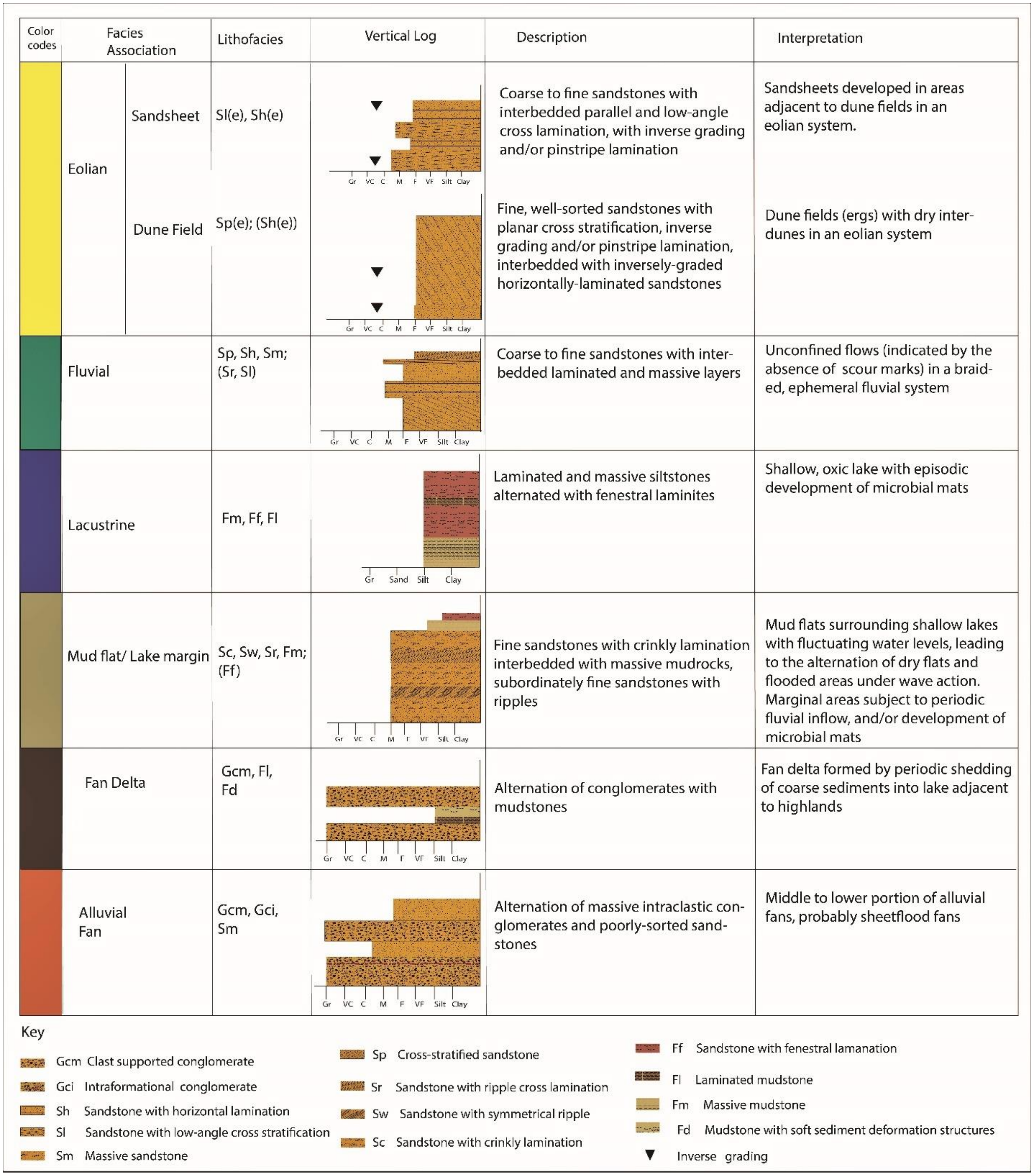

| Color codes | Facies Association | | Lithofacies | Vertical Log | Description | Interpretation |
|---|---|---|---|---|---|---|
| | Eolian | Sandsheet | Sl(e), Sh(e) | | Coarse to fine sandstones with interbedded parallel and low-angle cross lamination, with inverse grading and/or pinstripe lamination | Sandsheets developed in areas adjacent to dune fields in an eolian system. |
| | | Dune Field | Sp(e); (Sh(e)) | | Fine, well-sorted sandstones with planar cross stratification, inverse grading and/or pinstripe lamination, interbedded with inversely-graded horizontally-laminated sandstones | Dune fields (ergs) with dry inter-dunes in an eolian system |
| | Fluvial | | Sp, Sh, Sm; (Sr, Sl) | | Coarse to fine sandstones with inter-bedded laminated and massive layers | Unconfined flows (indicated by the absence of scour marks) in a braid-ed, ephemeral fluvial system |
| | Lacustrine | | Fm, Ff, Fl | | Laminated and massive siltstones alternated with fenestral laminites | Shallow, oxic lake with episodic development of microbial mats |
| | Mud flat/ Lake margin | | Sc, Sw, Sr, Fm; (Ff) | | Fine sandstones with crinkly lamination interbedded with massive mudrocks, subordinately fine sandstones with ripples | Mud flats surrounding shallow lakes with fluctuating water levels, leading to the alternation of dry flats and flooded areas under wave action. Marginal areas subject to periodic fluvial inflow, and/or development of microbial mats |
| | Fan Delta | | Gcm, Fl, Fd | | Alternation of conglomerates with mudstones | Fan delta formed by periodic shedding of coarse sediments into lake adjacent to highlands |
| | Alluvial Fan | | Gcm, Gci, Sm | | Alternation of massive intraclastic con-glomerates and poorly-sorted sand-stones | Middle to lower portion of alluvial fans, probably sheetflood fans |



Figure 4.6 : Description and interpretation of the established facies associations.

#### 4.1.2.2 Fluvial Facies Association

The Fluvial facies association comprises successions 1 to 10 feet thick, composed of coarse to fine sandstones, poorly to moderately sorted, with planar cross stratification (Sp), horizontal lamination (Sh) and/or massive (Sm), occasionally low angle cross stratification (Sl) (Figure-4.6). This facies association also occurs only in the lower sedimentary-dominated succession (Figure-4.7).

The abundance of tractive structures, poor sorting and overall fining-upward successions allowed the interpretation as channel deposits (Miall, 1977). The presence of planar cross stratification indicates sedimentation by currents under lower flow regime, while low-angle cross stratification and horizontal lamination indicates higher energy (transitional to upper flow regimes) in the depositional environment. The absence of scour surfaces at the base of successions suggests unconfined, shallow channels. Vertical successions with upper flow structures (Sh and Sl) at the base, grading to lower flow structures (Sp) indicate waning flows (Miall, 2006). This facies association is interpreted as ephemeral river deposits, formed by flashy discharge during flooding events.

#### 4.1.2.3 Lacustrine Facies Association

This facies association comprises 2-4 feet thick successions of laminated and massive siltstones (Fl and Fm), alternated with fenestral laminites (Ff) (Figure 4.6). It is only found at the top of the lower sedimentary-dominated succession and in the upper volcanic-dominated successions, in sections C and D (Figure-4.7).

The dominance of silt grain size, with minor mud fractions, indicates the low energy of the depositional environment. The absence of mudcracks and other structures indicative of subaerial exposure suggest a shallow, standing body of water. The fenestral laminites are interpreted as resulting from microbial activity in a lacustrine environment (Suarez-Gonzalez et al., 2019) where microbes bound and trapped the finer material onto microbial mats. Later desiccation formed the fenestrae filled by cement during diagenesis.

#### 4.1.2.4 Mudflat/ lake margin Facies Association

This facies association comprises an 11-feet thick sand body with crinkly lamination (Sc), interbedded with massive mudrocks (Fm), and subordinate rippled, fine sandstones with asymmetrical and symmetrical ripple cross laminations (Sr and Sw) (Figure-4.6). It occurs only in section B (Figure-4.7).

The dominance of fine grain sizes indicates deposition under low energy. An oxic environment is suggested by the abundant hematite staining. Crinkly laminations formed by microbial activity (Schieber et al., 2007) with interbedded Sw indicate fluctuations in the water level, with periodic displacement of the microbial mats by subaqueous, wave-reworked environments . The lack of evaporites and/or mudcracks suggests a wet/flooded, shallow open lake depositional environment surrounded by mud flats.

#### 4.1.2.5 Fan delta Facies Association

This facies association comprises 1-2 feet thick successions of dominantly clast supported massive conglomerate (Gcm), with minor laminated mudstone (Fl) and mudstone with soft sediment deformation (Fd) (Figure-4.6). It occurs only in the upper, volcanic-dominated succession (sections D and E) (Figure-4.7).

Deposition of matrix-supported, poorly sorted conglomerates (Gcm) results from viscous debris flows. The fine-grained intervals were deposited by suspension settling in a standing water body (Fl) where synsedimentary deformations occurred (Fd). Altogether, interbedding of these high-energy, proximal, gravity-flow deposits with fine-grained, subaqueous deposits suggests a proximal fandelta environment where the conglomeratic facies were deposited at the nearest submerged portion of the lake/river (Tamrakar et al., 2009).

#### 4.1.2.6 Alluvial fan Facies Association

This foot-thick rock body restricted within section-D only includes clast-supported massive conglomerates, clast-supported intraformational conglomerates and massive sandstones (Gcm, Gci and Sm, respectively) lithofacies (Figure-4.6). It occurs only in the upper, volcanic-dominated succession (sections D and E) (Figure-4.7).

The conglomerate facies represent subaerial debris flow deposits with lateral amalgamation of channel deposits. This nature of conglomeratic beds fining up to sandstone is indicative of stream channel alluvial fan deposit (Nichols, 2009).

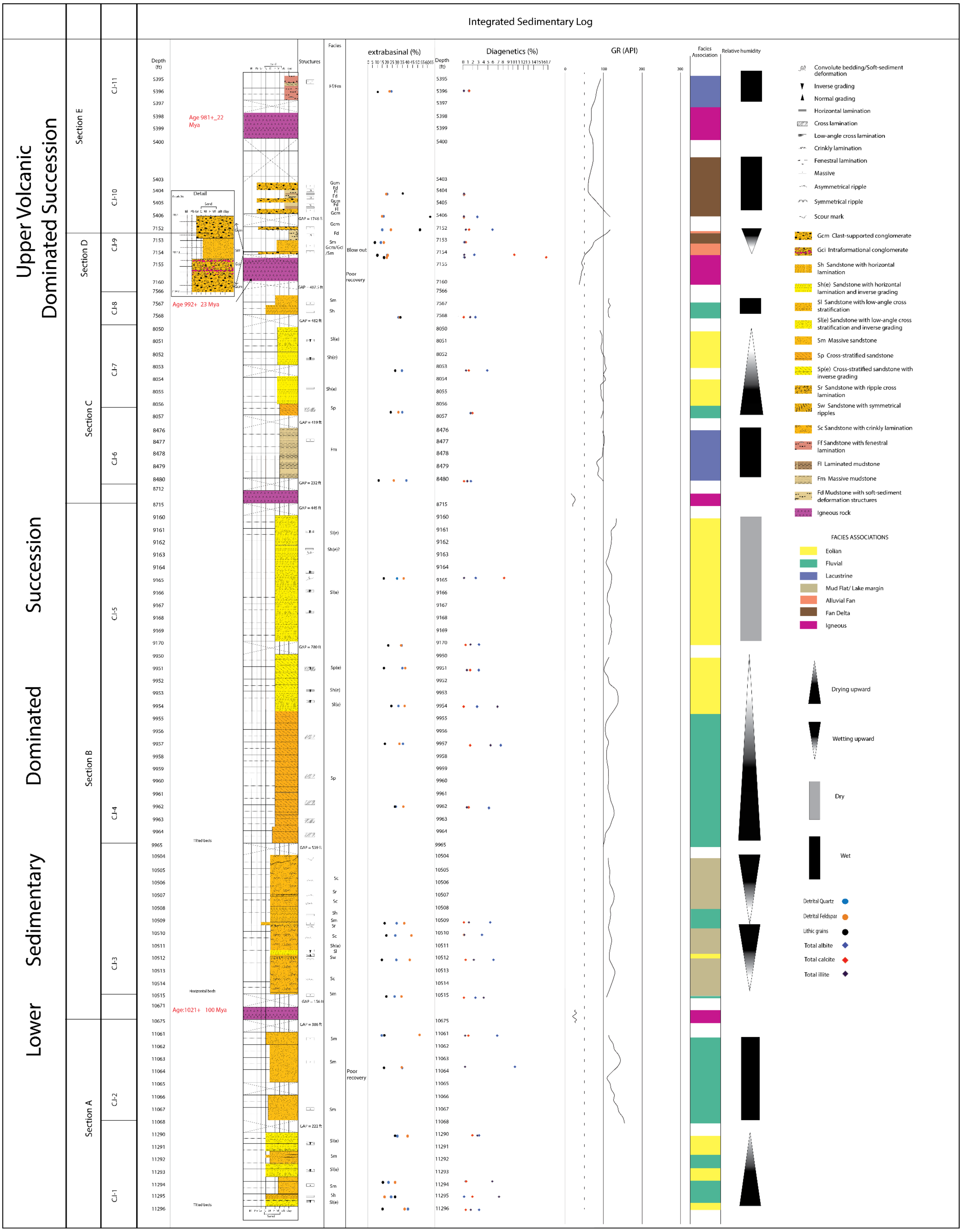

Figure 4.7 : Integrated sedimentary log, with the distribution of facies associations and vertical facies successions.

## 4.2 Provenance analysis

### 4.2.1 Quantitative petrographic analysis

Twenty-seven thin sections were quantified (Table-3.1). Texturally, they include very fine to very coarse sandstones, and subordinately pebbly conglomerates and siltstones (Figure-4.8). The grains are subangular to subrounded, with no apparent orientation in most samples, although imbricated, parallel, and chaotic orientation may occur in some samples. The sandstones vary from very poorly to well sorted, with some bimodal sandstones (Figure-4.9 A-C). The analyzed samples include sedimentary structures such as planar cross lamination, low-angle cross lamination, horizontal, and crinkly lamination (Figure-4.9 D-E), as well as inverse grading (Figure-4.9 F).

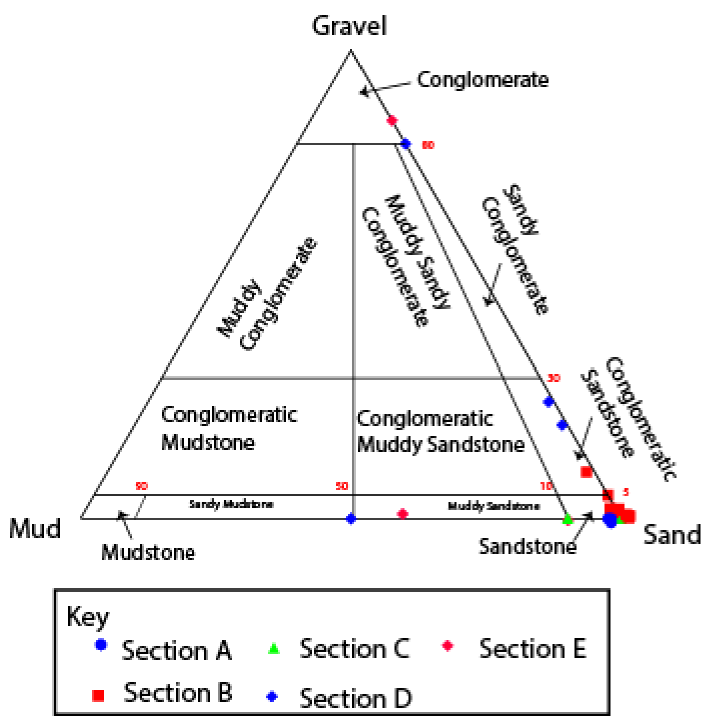


Figure 4.8 : Nomenclature used for mixtures of gravel, sand, and mud in sedimentary rocks (after Nichols, 2006), and the distribution of analyzed samples.

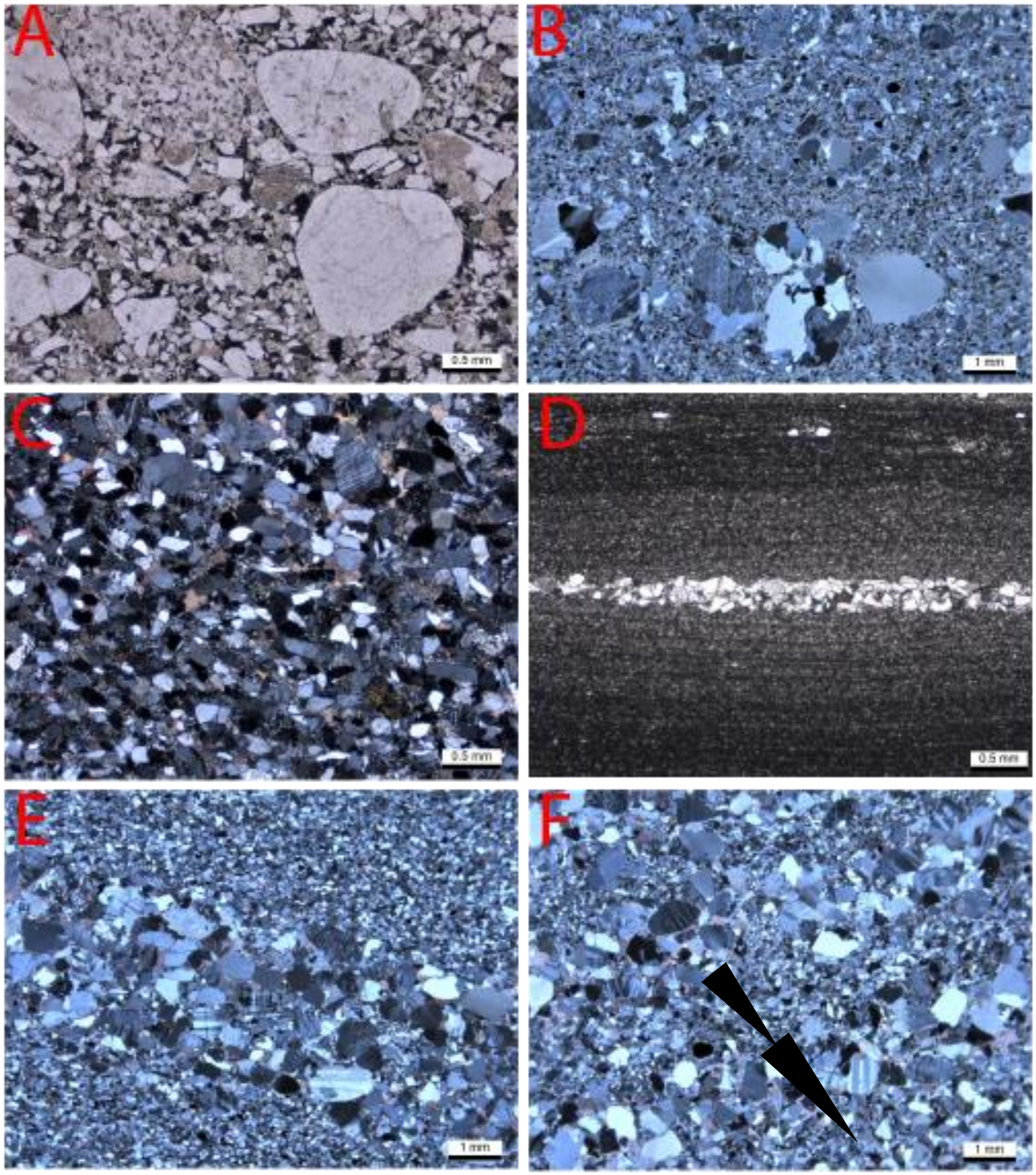


Figure 4.9 : Textures and structures of the quantified samples, A- very coarse- coarse, poorly-sorted sandstone; NP1 9170 feet; plane polarized light (PP), B- bimodal, fine-coarse poorly sorted sandstone; NP1 11295 feet, crossed polarizers (XP), C- medium, well-sorted sandstone; NP1 8056.6 feet; XP, D- laminated siltstone with fine sandstone interbeds; NP1 7153 feet; PP, E- low-angle cross stratification; NP1 11290 feet; XP, and F- low-angle cross lamination with inverse grading (inverted triangles); NP1 11296 feet; XP.

Compositional analysis included primary and diagenetic constituents. The original composition is feldspatho-lithic, with mostly lithic arkoses and feldspathic litharenites, and subordinately arkoses (sensu McBride 1963, Figure-4.10). The percentages for quantified primary constituents for each core section are summarized in Table-4.1. Also, Figure-4.7 shows the distributions and quantification data of the analyzed samples, with both the primary and diagenetic constituents.

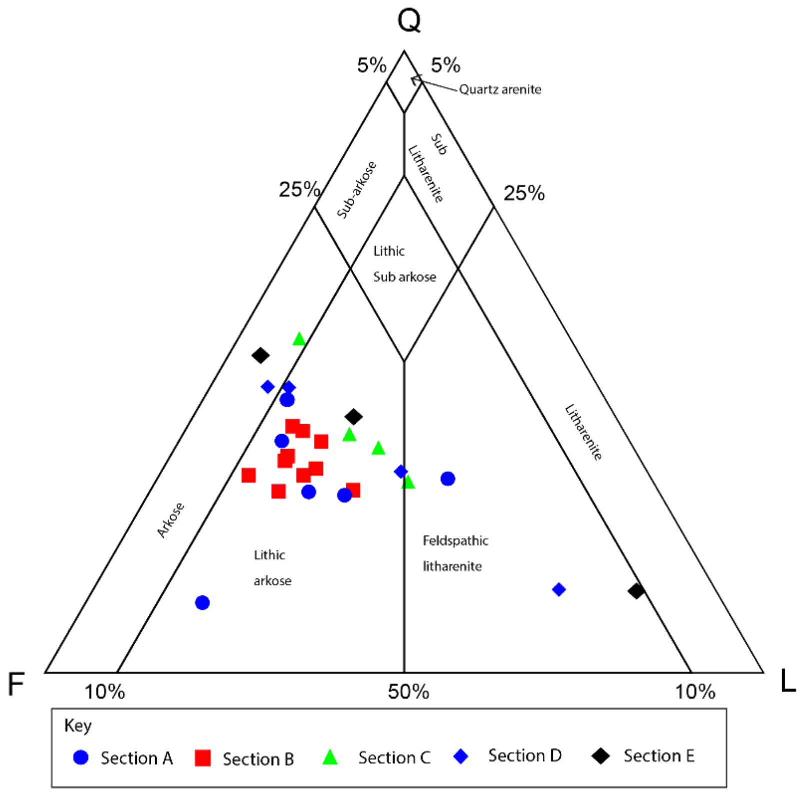


Figure 4.10 : Detrital composition of the samples in NP#1 plotted in McBride (1963) diagram (Q- quartz, F- feldspar and L- lithics).

The average quartz-feldspar-lithics ratio in Section A determined from six thin sections is $Q_{33}F_{45}L_{22}$, where the quartz is mostly monomineralic, with minor polycrystalline grains (Figure-4.11 A). The amount of K-feldspar exceeds that of plagioclase, 75%, and 25%, respectively.

The feldspars are highly altered in most of the samples. Lithic fragments include abundant plutonic and metamorphic rock fragments in every sample, with a dominance of infracrustal rock fragments compared to the supracrustal lithics (volcanic and sedimentary rock fragments ). Similar trends are observed in the overlying section as well.

In Section-B, analysis of 10 thin sections collected in different core intervals and facies resulted in an average $Q_{36}F_{45}L_{19}$, roughly similar to Section A, where monocrystalline quartz is abundant (Figure-4.11 B). Similarly, K-feldspar exceeds plagioclase, 78% and 22% respectively, with slight to highly alterations. Lithics mostly include plutonic and metamorphic rock fragments, with a slight increase in the amount of metamorphic and volcanic fragments compared to previous section, although the higher ratio of infracrustal to supracrustal fragments is similar to Section A.

Four thin sections from three core intervals represent Section C. The average $Q_{42}F_{33}L_{25}$ indicates that both quartz and lithic fragments are significantly higher relative to sections A and B. Monomineralic quartz is abundant, with rare polycrystalline quartz, and the feldspars include mostly K-feldspar (slightly to highly altered) compared to plagioclase, 77% and 23%, respectively (Figure-4.11 C). In terms of lithic fragments, infracrustal fragments are higher than supracrustal ones. The abundance of metamorphic rock fragments is higher, although plutonic rock fragments remain the dominant lithics, 42%, and 48%, respectively. The abundance of volcanic rock fragments is slightly lower than in Sections A and B, and no sedimentary rock fragments were noted in any of the samples.

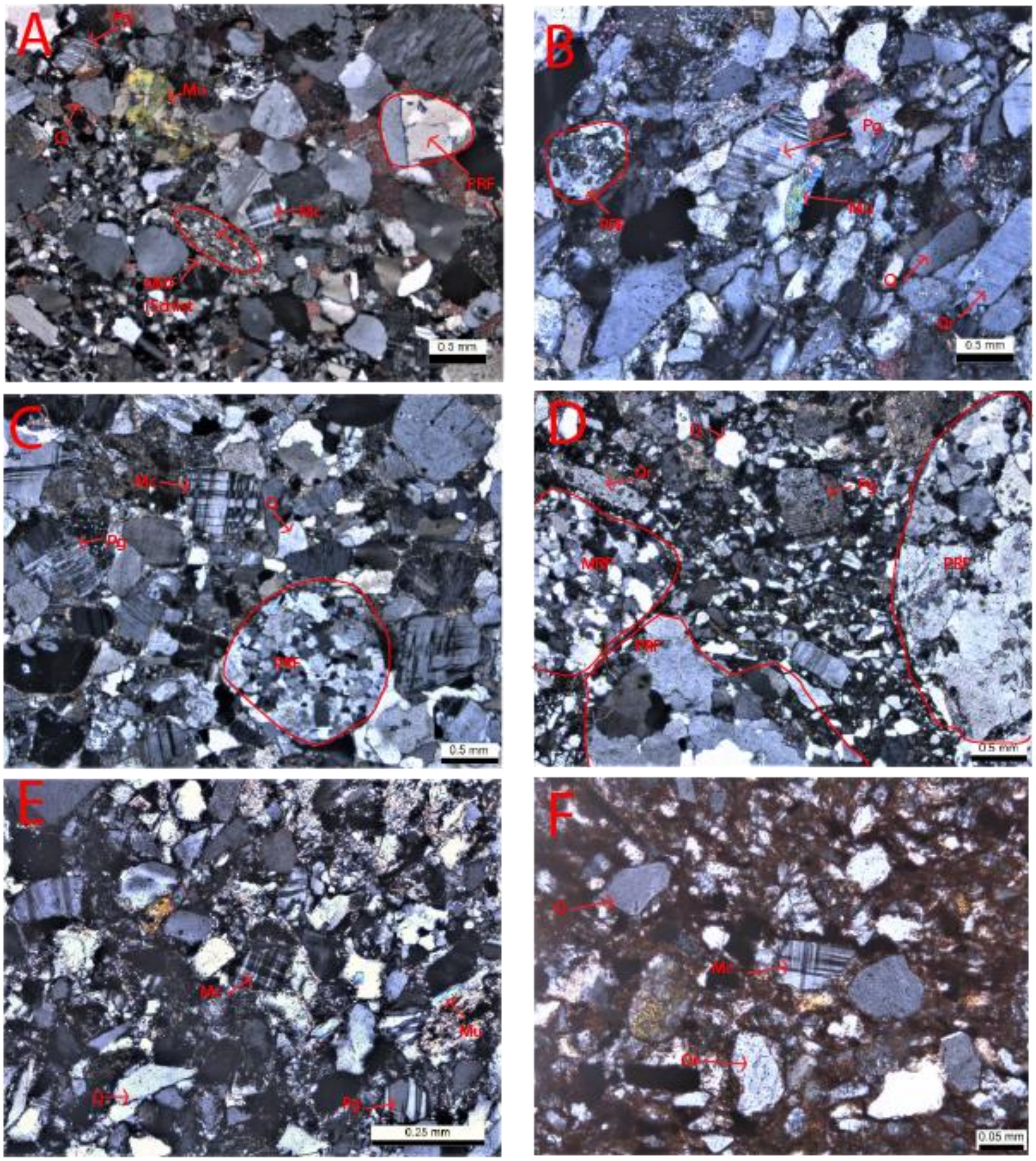


Key Q-Quartz, Pg-Plagioclase feldspar, Mc- Microcline, Or- Orthoclase, Mu-Muscovite, PRF- Plutonic Rock Fragment, MRF-Metamorphic Rock Fragment, VRF-Volcanic Rock Fragment

Figure 4.11 : Composition of the quantified samples, A- Lithic arkose; NP1 11290 feet; Section A; crossed polarizers (XP), B- Lithic arkose; NP1 10509 feet; Section B; XP, C- Feldspathic litharenite; NP1 7568 feet; Section C; XP, D- Feldspathic litharenite; NP1 7152 feet; Section D; XP, E- Arkose; NP1 8480 feet; Section D; XP, F- Arkose; NP1 5396 feet; Section E; XP.

The remaining samples are taken from the volcanic-dominated succession. Seven thin sections from three different core intervals represent sections D and E. Four samples from core interval 9 (Section-D) display $Q_{29}F_{28}L_{43}$, showing a shift towards a higher contribution of lithics compared with the underlying sections. Quartz is monocrystalline only. The feldspars are slightly altered, and K-feldspars are more abundant than plagioclase, 69% and 31%, respectively. Abundant lithic fragments are observed (Figure-4.11 D-E), mostly plutonic, with minor metamorphic, and rare volcanic rock fragments. Hence the supracrustal contribution is significantly lower than infracrustal, similar to the sedimentary-dominated succession below.

Likewise, three samples from Section E show average $Q_{29}F_{25}L_{46}$, with abundant lithic fragments. However, the samples were taken from different facies, both coarse and fine-grained facies. Therefore, a facies-dependent shift is observed in the QFL ratio. The coarse-grained sample, NP1-5406, with $Q_{13}F_{11}L_{76}$, has abundant lithic fragments, mostly plutonic rock fragments (95%). The other two, fine-grained samples have average $Q_{46}F_{42}L_{12}$, indicating an abundance of quartz and feldspar. Monomineralic quartz and higher K-feldspar (75%) to plagioclase ratio have been observed (Figure-4.11 E). Despite the low abundance of lithics in these samples, plutonic rock fragments are still higher than other lithic types.

Accessory mineral assemblages from the study include opaque minerals in most of the samples, followed by muscovite and some heavy minerals such as pyroxene, rutile, zircon, tourmaline, and epidote. The average abundance of opaque minerals is up to 2% (maximum up to 4%) in all core intervals, except for the sample in core interval 11, which contains 8% of opaque minerals. Heavy minerals account for less than 1% in most samples, except for core intervals 1 and 3, which show maximum values up to 3%.

Table 4-1 : Calculated averages and maxima of primary constituents for the quantified thin sections in different core sections. Modal grain size in mm, numerical sorting (dimensionless), and extrabasinal constituents in percentage (lithics include PRF- plutonic rock fragments, MRF- metamorphic rock fragments, VRF- volcanic rock fragments, SRF- sedimentary rock fragments).

| | Section A | | Section B | | Section C | | Section D | | Section E | |
|---|---|---|---|---|---|---|---|---|---|---|
| | Average | Maximum | Average | Maximum | Average | Maximum | Average | Maximum | Average | Maximum |
| Modal grain size (mm) | 0.5 | 0.8 | 0.3 | 0.4 | 0.5 | 1.5 | 1.5 | 6.0 | 2.0 | 6.0 |
| Numerical sorting | 0.7 | 1.0 | 0.7 | 1.0 | 0.50 | 0.6 | 1.5 | 2.2 | 1.3 | 2.2 |
| Extrabasinal constituent | | | | | | | | | | |
| Detrital quartz | 21.5 | 35.0 | 26.3 | 31.3 | 30.9 | 34.7 | 10.8 | 14.7 | 15.4 | 19.7 |
| Detrital feldspar | 28.9 | 46.0 | 33.0 | 40.7 | 25.2 | 29.3 | 10.7 | 14.7 | 13.6 | 17.3 |
| Total K-feldspar | 21.7 | 32.3 | 25.6 | 30.3 | 19.6 | 23.3 | 7.4 | 10.3 | 10.1 | 13.3 |
| Total plagioclase | 7.2 | 13.7 | 7.4 | 10.3 | 5.7 | 6.7 | 3.3 | 4.7 | 3.4 | 4.0 |
| Lithics | 13.9 | 22.0 | 14.2 | 22.7 | 19.5 | 30.3 | 16.5 | 49.3 | 24.6 | 64.7 |
| MRF | 0.9 | 2.3 | 2.6 | 5.7 | 8.2 | 13.0 | 1.8 | 4.7 | 0.6 | 1.3 |
| PRF | 11.7 | 17.3 | 10.1 | 16.3 | 9.4 | 20.7 | 13.1 | 43.0 | 23.4 | 61.7 |
| VRF | 1.0 | 3.3 | 1.5 | 4.3 | 1.9 | 4.3 | 1.6 | 2.3 | 0.6 | 1.7 |
| SRF | 0.3 | 1.7 | 0.0 | 0.3 | 0.0 | 0.0 | 0.0 | 0.0 | 0.0 | 0.0 |

Among the diagenetic constituents, albite is the most abundant, being present in all the thin sections in variable amounts. Albite occurs as overgrowths on feldspar (Figure-4.12 A), as well as replacing both the monomineralic feldspar (Figure-4.12 B) and feldspars in rock fragments. The percentages for quantified diagenetic constituents for each core section are summarized in Table-4.2. Average albite content varies from 1 to 4% for the different core intervals (maxima 2-10%), but no trends or systematic variations were detected. Sections A and B have the highest amount of albite reported, with an average of approximately 4%, decreasing upsection.

Calcite is the second most abundant diagenetic constituent. Microcrystalline and coarsely crystalline non-ferroan calcite occurs as a cement, coating the primary grains and filling intergranular pores and/or replacing other diagenetic minerals, such as albite overgrowths (Figure-4.12 C). It also fills rock fractures, along with diagenetic silica and rarely ferroan calcite (Figure-4.12 D, E) in Section B. Finally, it also fills zeolite-lined fenestrae in Section E (Figure-4.12 F). Calcite abundance varies considerably, with averages between zero and 2% in all the sections, except for Section D (average 7%, maximum 16%).

Illite occurs mostly as fibrous crystals filling intergranular pores and coating the grains (Figure-4.13 A), occasionally replacing primary grains. It is present in samples from the lower sedimentary-dominated sequence (sections A, B, C), with averages up to 3% (maxima up to 7%); its abundance decreases upwards and it is absent in the upper volcanic-dominated sequence.

The opposite occurs in relation to diagenetic iron oxide/hydroxides, which is abundant in the upper sections (average 15-30%, maxima 31-38% in sections D and E) and absent in the lower sections. Microcrystalline Fe oxides/hydroxides replace the detrital matrix and other diagenetic minerals (Figure-4.13 B).

Table 4-2 : Calculated averages and maxima of diagenetic constituents for the quantified thin sections in different core sections. Modal grain size in mm, numerical sorting dimensionless, and diagenetic constituents in percentage.

| | Section A | | Section B | | Section C | | Section D | | Section E | |
|---|---|---|---|---|---|---|---|---|---|---|
| | Average | Maximum | Average | Maximum | Average | Maximum | Average | Maximum | Average | Maximum |
| Modal grain size (mm) | 0.5 | 0.8 | 0.3 | 0.4 | 0.5 | 1.5 | 1.5 | 6 | 2 | 6 |
| Numerical sorting | 0.73 | 1.00 | 0.66 | 1.00 | 0.5 | 0.6 | 1.43 | 2.2 | 1.00 | 1.00 |
| Diagenetic constituents | | | | | | | | | | |
| Total albite | 3.89 | 10.33 | 4.062 | 7.34 | 2.4175 | 4.66 | 1.92 | 5.67 | 1.23 | 2.67 |
| Total calcite | 0.78 | 1.66 | 1.232 | 8 | 0.6675 | 1.67 | 6.92 | 16.34 | .33 | 1.00 |
| Total illite | 2.78 | 7.00 | 2.17 | 6.67 | 0.915 | 1.33 | 0.08 | 0.33 | 0 | 0 |
| Total Fe Oxide//Hydroxides | 0 | 0 | 0 | 0 | 2 | 8.00 | 11.5 | 33.67 | 24 | 38.33 |
| Total Ti minerals | 0 | 0 | 1 | 3.99 | 1.17 | 2.67 | 4.33 | 16.00 | 0 | 0 |
| Total epidote | 0.06 | 0.33 | 0.332 | 1.66 | 1.25 | 2 | 3.41 | 8.00 | 1.11 | 1.67 |

Similarly, diagenetic titanium minerals occur only in the uppermost part of Section B, and in sections C and D, with an average abundance of between 1 and 3% (maxima 2-16%). Microcrystalline titanium minerals fill intergranular pores (Figure-4.13 C), while coarsely crystalline titanium minerals replace both primary constituents and other diagenetic minerals.

Minor amounts of microcrystalline and prismatic epidote replace detrital grains and other diagenetic components (Figure-4.13 D). Except for Section D (average 3%, maximum 8%), all other sections display maximum abundance of epidote of less than 2%. Microcrystalline and vermicular chlorite, the latter filling rock fractures, accounts for less than 1% of the mode (Figure-4.13 E, F).

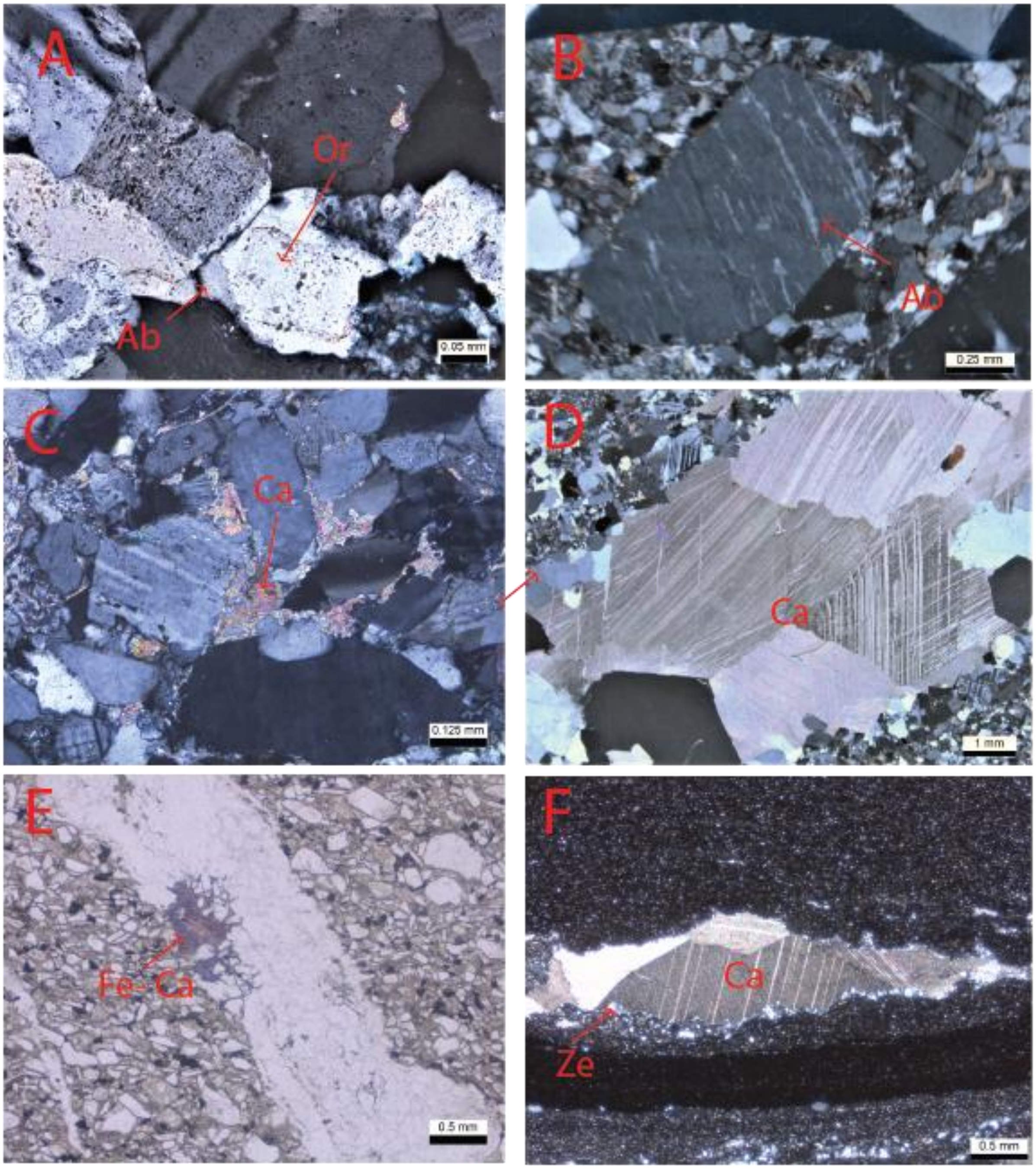


Figure 4.12 : Diagenetic constituents identified in thin sections from NP#1; A- Albite overgrowths covering feldspars; NP1 11063.5; Section A; XP, B- Albite replacing orthoclase; NP1 11296; Section A; XP, C- Calcite filling intergranular pores and replacing albite overgrowths; NP1 10515; Section B; XP, D- Coarsely-crystalline calcite in rock fracture; NP1 9164.7; Section B; XP, E- Ferroan calcite replacing diagenetic silica in rock fracture; NP1 11295; Section A; PP, F- Calcite filling fenestrae lined with zeolite; NP1 5404.2; Section E; XP.

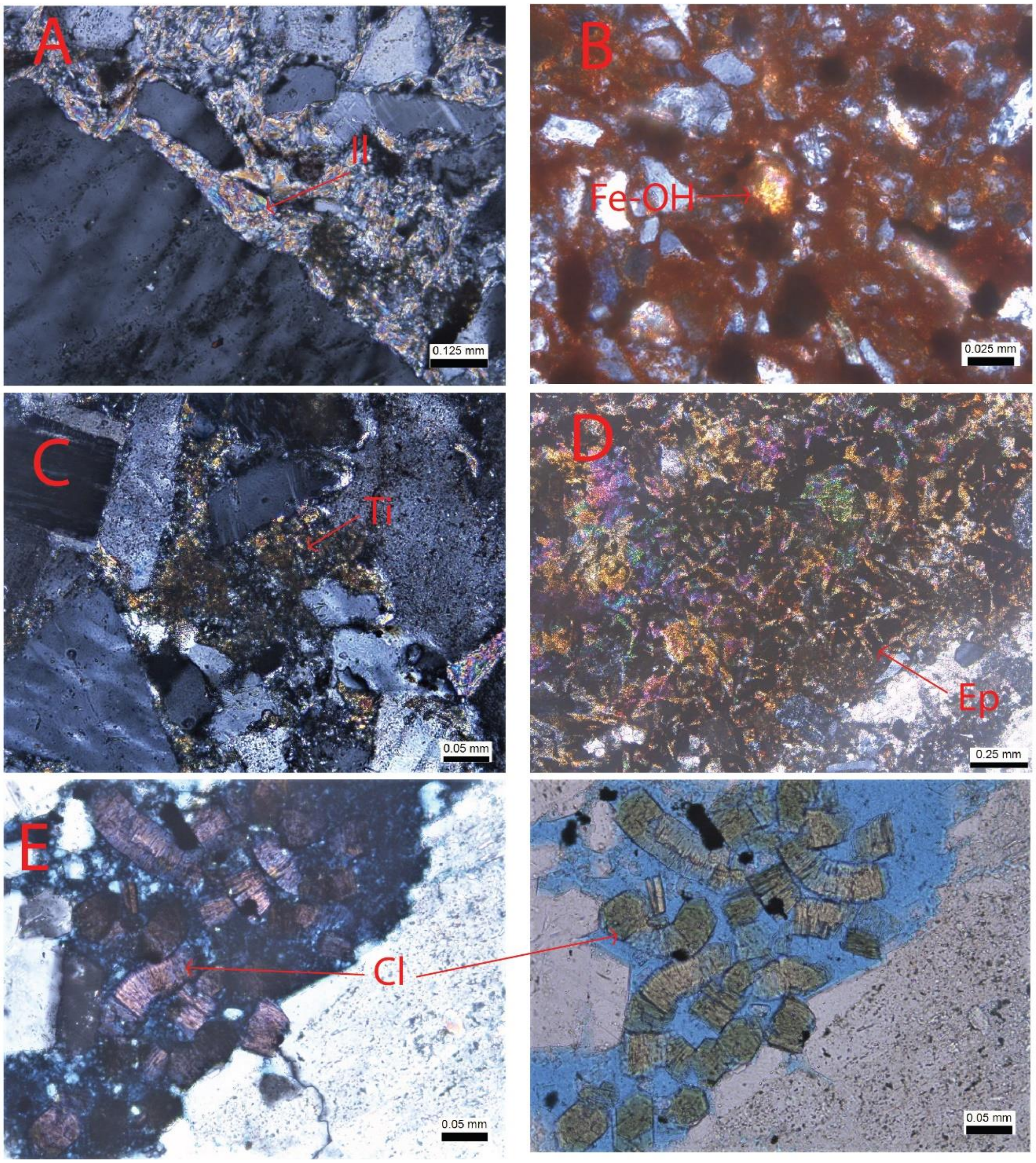


Key
Il-illite , FE-OH- iron oxide/ hydroxide, Ti- diagenetic titanium mineral, Ep- diagenetic epidote, Cl- chlorite

Figure 4.13 : Diagenetic constituents identified on thin sections from NP#1; A- Illite cement, lining detrital grains and filling the pores; NP1 10510; Section B; XP, B- Iron oxide/hydroxide replacing detrital matrix and illite; NP1 7154.2; Section E; XP, C- Microcrystalline titanium mineral filling intergranular pores; NP1 7154; Section E; XP, D- Prismatic epidote replacing other diagenetic constituents; NP1 7154.2; Section E; XP, E and F- Vermicular chlorite engulfed by diagenetic silica in rock fracture; NP1 11061; Section A; XP and PP, respectively.

### 4.2.2 Provenance analysis and interpretation

Quantitative data on primary composition shows that the analyzed samples display two main groups in a ternary plot of quartz-feldspar-lithics (Figure-4.10).

The samples from Sections A and B, in the lower sedimentary-dominated succession (i.e. depths 11068-8050 ft), show less variation in terms of composition, falling mostly in the lithic arkose and feldspathic litharenite fields (Figure-4.10). On the other hand, samples from Section C, in the lower sedimentary-dominated succession, and Sections D and E, in the upper volcanic-dominated succession, show compositions ranging from arkose, lithic arkose, to feldspathic litharenite. This manifests changes in sediment sources due to re-arrangement of the tectonic blocks and amalgamation of new active feeder system (Arribas et al., 2003).

The Dickinson I provenance diagram (Figure-4.14) shows that the majority of samples originated from uplifted continental basement. Most exceptions to this observation are samples from section C. Four samples taken from Section C show a variable provenance ranging from continental basement uplifted to transitional continental setting to dissected magmatic arc. This observation seems to comply with the general set up of extensional basin where lithic-poor, quartzofeldspathic sands derive from fault-bounded basement uplifts and eroded plutons in deeply dissected magmatic arcs (Dickinson, 1985).

The provenance diagram (Figure-4.14) shows that sediment sources change from uplifted basement block (Section A and B) to transitional continental and magmatic arc settings (Section C) and then back to uplifted basement block (Section D and E).

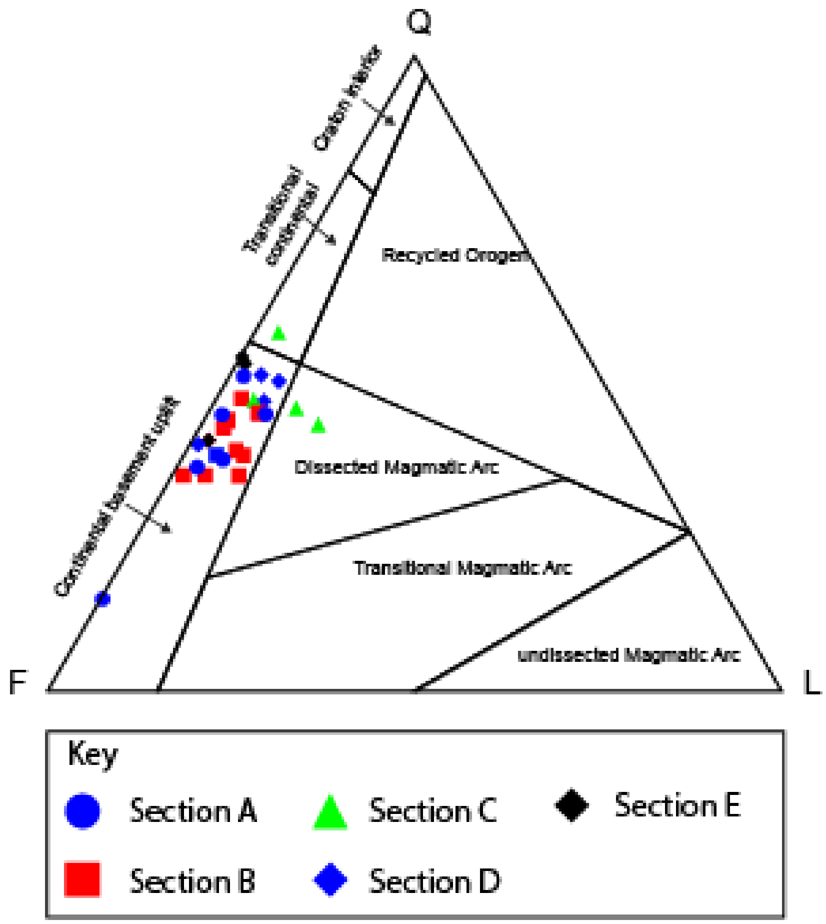


Figure 4.14 **:** Distribution of the studied samples in the provenance Dickinson I diagram (Dickinson, 1985).

# Chapter 5 - Discussion

The limited availability of cores from Texaco Noel Poersch#1 poses a limitation for this study. To minimize that, wireline log data have been used. For example, gamma-ray signature was used to distinguish between volcanic and sedimentary rocks. Also, the composite well log made from combining wireline log and well cuttings data were helpful to predict the lithologies in the well. However, despite providing an approximate lithological data, the composite well log did not provide any information pertaining to facies in the sedimentary succession, essential to infer the depositional processes and interpret depositional environments. Therefore, the depositional model proposed below did not take into account intervals with missing cores.

## 5.1 Depositional model

The facies analysis of the rocks from the Texaco Noel Poersch#1 well shows that the rocks are indicative of six different facies associations, described and illustrated in Figure-4.4 and 4.5. The evolution of these facies associations in time provides the basis for an evolutionary depositional model. The depositional snapshots (Figures 5.1-5.5) described below represent the depositional environments in which the units in Noel Poersch#1 were deposited, from base to top, Sections A, B, C, and D (Figure-4.5).

At the very bottom of the well, within core interval 1 (11296-11290 ft), repetitive occurrence of eolian and fluvial facies associations is observed, with an overall thickening-upward trend of the eolian  facies association, suggesting a drying-upward interval. This is followed by a 6 ft thick fluvial deposit in core interval 2 (11068-11061 ft), indicating a wetter period, eventually topped by a 218 ft thick basalt (identified from gamma-ray log). These two discontinuous core internvals comprise Section A, which shows the alternating nature of dry and wet climates.

This interpretation suggests that Section A (11296-11061 ft), the lowermost in the well, was deposited by axial fluvial systems (Leeder and Gawthorpe, 1987) within the half-graben basin formed by rifting (Figure-5.1). Ages obtained in the overlying basalt (1021±100 My) indicate deposition in the Proterozoic (Berendsen, 1997). Proterozoic rivers were braided systems, as a consequence of the lack of vegetation and poor soil development to provide bank stability (Eriksson et al., 1998; Sønderholm & Tirsgaard, 1998, Bose et al., 2012). This agrees with the absence of mudrocks (both in the cores and un-cored intervals, as identified from wireline log data), and dominance of coarse to medium-sand grain size in Section A, typical of bedload-dominated, braided river deposits (Miall 1977, 1978). The fluvial system is interpreted as having developed along the axial zone on the downfaulted block, as suggested for asymmetrical half-graben basins, where channels tend to occupy the axis of maximum subsidence (Bridge and Leeder, 1979). Laterally adjacent to it, wind reworking allowed the development of dune fields. Alternatively, rather than concomitant with the fluvial system, the dune fields could have been developed intermittently, in response to wind reworking of ephemeral fluvial sediments during dry periods.

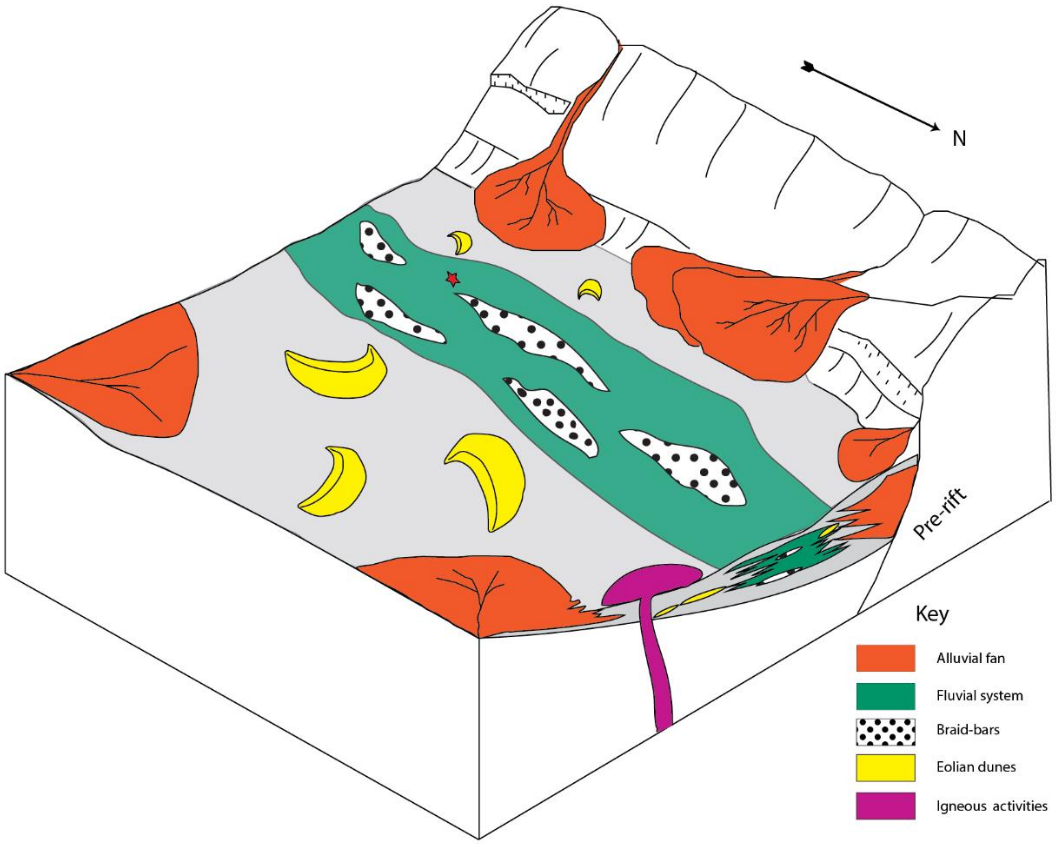


Figure 5.1 : Depositional model proposed for Section A. The red star marks the approximate location of NP#1 well.

Avulsion of the axial river is a very common phenomenon in continental half-grabens due to episodic tectonic tilting (Leeder and Gawthorpe, 1987). Rearrangement of tectonic blocks in the rift basin may result in lateral shifts of the fluvial system, resulting in interbedded fluvial and eolian deposits (Figure-5.1). Provenance data suggest that uplifted basement blocks served as the sediment source, with the detrital composition ranging from arkose, lithic arkose to feldspathic litharenite, suggesting multiple source areas. This stage of evolution ended with volcanism that resulted in the extrusion of 218 ft thick flood basalts, estimated from the gamma-ray signature (Figure-2.4).

The vertical facies succession suggests that Section B contains core intervals that record at least two different depositional systems, from base to top, sections B-1 and B-2, respectively.

Section B-1 (10515-10504 ft) contains mostly mudflat/lake margin deposits, with a minor interbed of eolian and a foot-thick fluvial deposit, marking two wetting-upward cycles. The base of Section B-1 is a flooding surface (FS1) that separates fluvial-eolian deposits (Section A) from dominantly marginal lake deposits in Section B-1. A flooding surface denotes transgression due to the rise of base level (Catuneanu et al., 2011), where base level is the surface to which sediment accumulation fills up to or erodes down to. In this study, the flooding surfaces were identified by the superposition of facies associations indicative of increasing base level (e.g. marginal lake overlying eolian facies associations). The depositional model shows back-stepping of the fluvial systems and expansion of a lake (Figure-5.2), reflecting an increase in the accommodation to sediment supply ratio. The presence of eolian dunes adjacent to the lake is related to variations in the water level in response to local or global fluctuations (controlled by climate and/or tectonics). Traversal systems are inferred from the assumption that elevated rift shoulders/hanging wall blocks favor the development of alluvial fans, as these are very common in rift basins (Leeder and Gawthorpe, 2000).

Following a gap of about 539 ft above Section B-1 (that, based on well cuttings data appears to be composed mostly of sandstones), Section B-2 (9965-9950 ft) is characterized by the return of fluvial and eolian systems in the basin, and thus marks a drying-upward interval, with the transition to arid climate (Figure-5.3). The presence of tilted beds in Section B-2 points to reorientation of blocks in response to tectonic episodes. Sedimentary supply was derived from uplifted basement blocks with fairly uniform (lithic arkose) composition, suggesting a single source (rather than multiple sources as in Section A). The top of Section B-2 (9170-9160 ft) is characterized by the persistence of eolian systems.

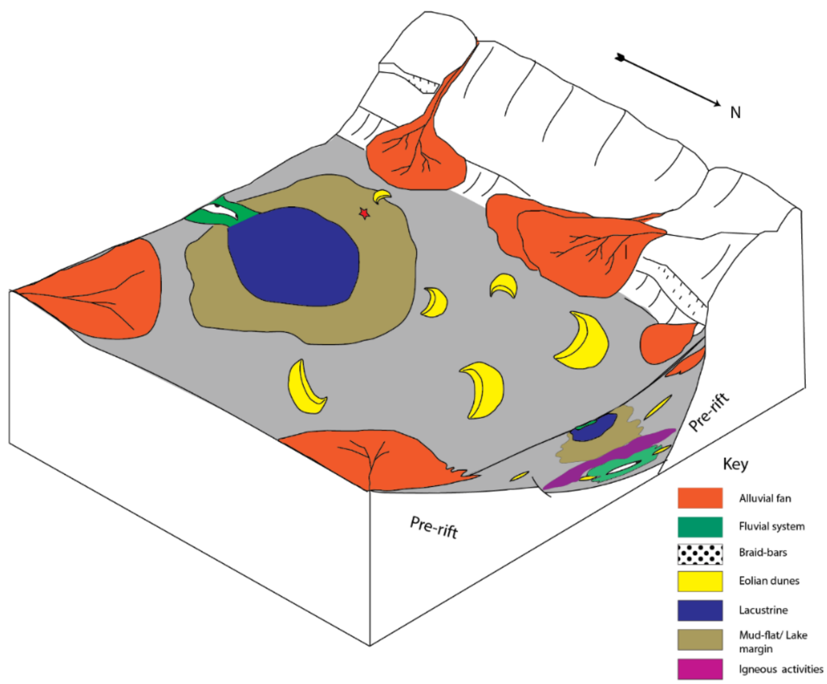


Figure 5.2 : Depositional model proposed for Section B-1. The red star marks the approximate location of NP#1 well.

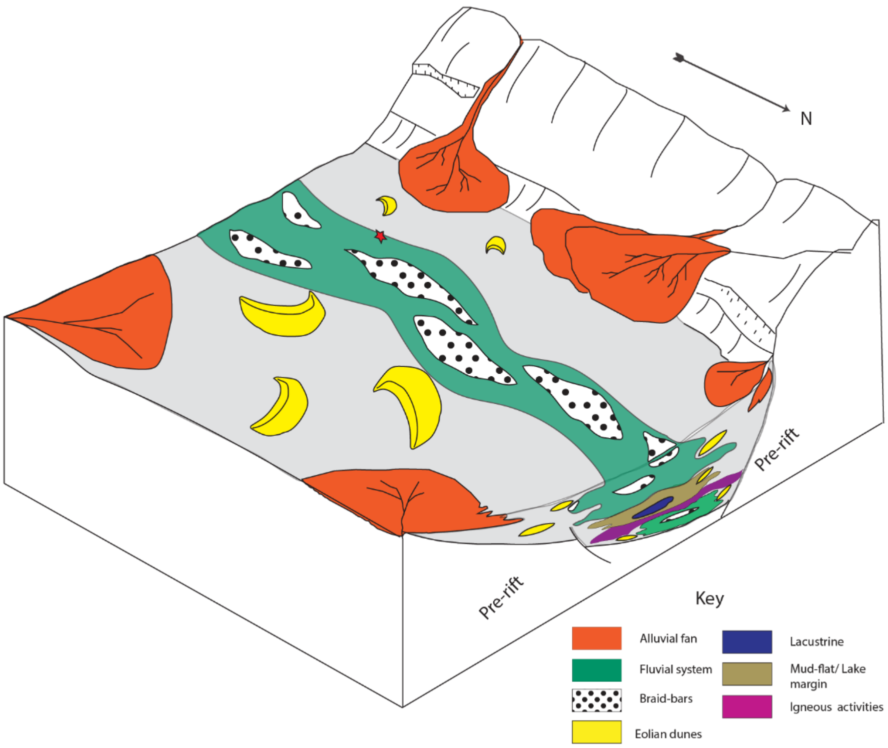


Figure 5.3 : Depositional model proposed for Section B-2. The red star marks the approximate location of NP#1 well.

The gap of 730 ft between core interval 4 and core interval 5 makes it impossible to affirm that the eolian systems persisted uninterruptedly, since there is no rock data. The end of Section B was marked by another intense episode of igneous activity, resulting in the accumulation of 134 ft of basalt.

Section C comprises lacustrine deposits at the base (in core interval 6), which represent the second flooding surface (FS2), since it overlies the eolian deposits of Section B-2, thus representing a rise on the base level that marks a transgression, followed by fluvial-eolian deposits (in core intervals 7 and 8). This marks a wet period that later gives way to arid conditions, marking a drying-upward interval from core interval 6 to core intervals 7-8, respectively. With a gap of 492 ft between core interval 6 and core interval 7, it is difficult to pin down how the change in depositional systems took place, and hence the paleogeographic reconstruction in Figure-5.4 focuses on the dominance of lacustrine systems in the rift basin, assuming the possibility that eolian systems existed adjacent to them. The vertical succession in Section C is similar to the one observed in Section B, where lacustrine systems at the base give way to fluvial-eolian systems at the top.

The overlying units are part of the upper volcanic-dominated succession. Following a gap of 407.5 ft, the presence of basalt at the base of core interval 9 points to renewed igneous activities and associated changes within the basin in Section D. Overlying the basalt, alluvial fan deposits indicate the progradation of proximal systems (Figure-5.5). The replacement of alluvial fan by fan delta deposits marks a flooding event in the basin (FS3) during the deposition of core interval 9, and thus a wetting-upward cycle. Fan delta systems persisted through the beginning of Section E (core interval 10), with intense igneous activity that led to extrusion of basalts. The lacustrine deposits in Section E (core interval 11), overlying the basalts, mark the fourth flooding surface in the studied succession (FS4), indicating the return of wet climate.

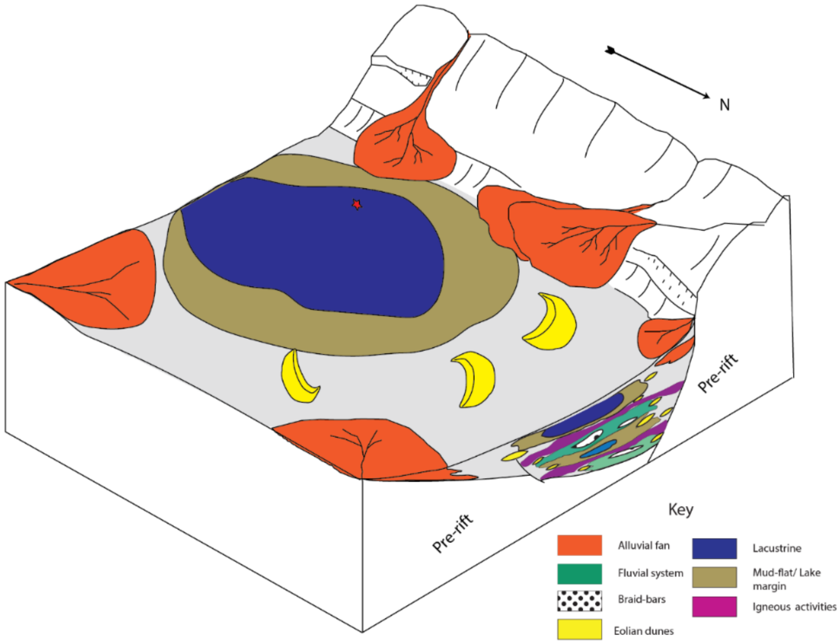


Figure 5.4 : Depositional model proposed for Section C. The red star marks the approximate location of NP#1 well.

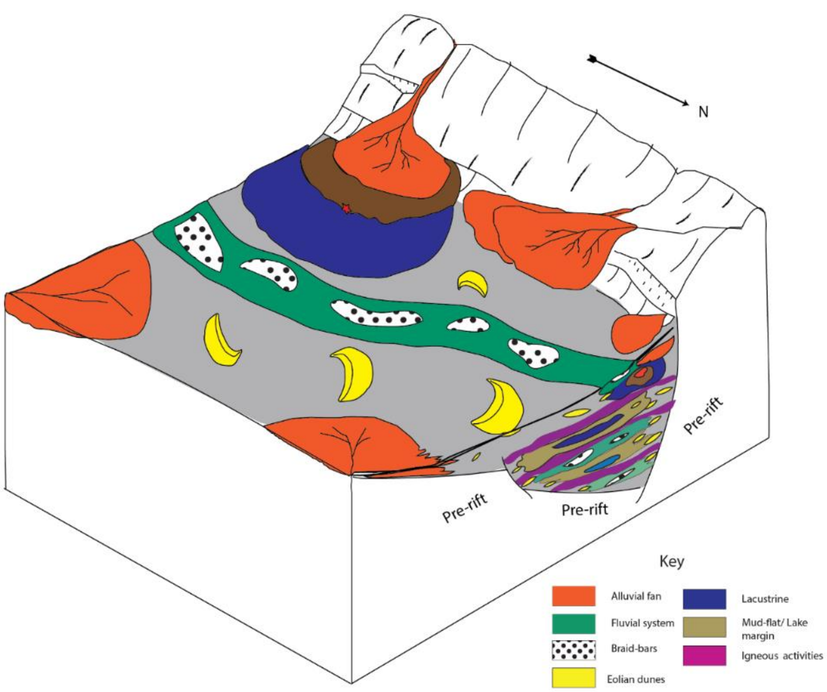


Figure 5.5 : Depositional model proposed for Section D. The red star marks the approximate location of NP#1 well.

Variations in provenance, such as the ones identified in this study, may be related to re-organization of the drainage basin and/or erosional unloading to the rift shoulder causing an uplift (Burov and Cloetingh, 1997). The increasing compositional variation in the analyzed samples also suggests diversification of the sediment sources, with more uniform composition in Sections A and B and a more varied composition in Sections C, D and E.

## 5.2 Stratigraphic framework

Section 5.1 describes cyclic behavior of facies associations within the Mid-continent rift basin. Identification of flooding surfaces can be used to establish a sequence stratigraphic framework in which rift sequences, bounded by flooding surfaces, are internally composed of systems tracts based on stacking patterns. Such stacking patterns are a function of accommodation and sediment supply Martins-Neto and Catuneanu (2010). This sequence-stratigraphic model for rift basins includes three phases within a sequence, starting with an underfilled phase characterized by high accommodation to sediment supply ratio. This is followed by a filled phase where there is relative balance between accommodation and sediment supply. The sequence is topped by an overfilled phase in which sediment supply exceeds accommodation. As the rifting progresses, the episodic nature of rift-related tectonic events leads to subsidence and the cycle starts again. Flooding surfaces are, therefore, used as key surfaces for sequence boundaries, since rapid generation of accommodation results in transgression in an underfilled phase, such as a lacustrine setting (Martins-Neto and Catuneanu, 2010).

Following this concept, three rift sequences, composed of an underfilled systems tract at the base and an overfilled systems tract at the top, have been identified within the cored intervals. Differently from the sequences that compose the model proposed by Martins-Neto and Catuneanu (2010), no balanced systems tract (where accommodation is in balance with sediment supply, resulting in thick coarse-grained intervals alternated with thin fine-grained ones) was identified, perhaps due to the discontinuous nature of the cored intervals. Sequence-1 (Seq. 1) is bounded at the base by flooding surface 1 at 10515 ft, with an underfilled phase that switches towards an overfilled phase at 9160 ft, marking the transition from high to low accommodation/sediment (Figure-5.6). The next sequence (Seq. 2) is marked at the base by flooding surface 2 at 8480 ft and continues until 7566.5 ft, following the same underfilled-overfilled phases. Seq. 3 is marked at base by flooding surface 3 at 7153 ft and at the top by flooding surface 4 at 5397 ft (Figure-5.6). However, lack of data for a considerable depth (1746 ft) prevents us from making inferences on the continuation of this sequence. Gamma-ray log signatures indicate a thick mafic extrusion from 7130-5700 ft.

Apart from these three rift sequences, the topmost core interval records flooding surface 4, which could be the base of a new sequence, followed by an underfilled phase (core interval 11). Likewise, the bottommost part from Section A (C.Is 1-2) could represent the overfilled phase of a prior rift sequence. However, such speculation could not be confirmed due to lack of data.

The stratigraphic analysis led to the identification of repetitive transgression and regression cycles. At the base (11296-10504 ft), fluvial and eolian facies associations are replaced by lacustrine and mudflat ones, forming a transgressive cycle. Between 9965 ft and 8050 ft, a transgressive-regressive cycle is represented by fluvial and eolian facies associations, overlain by lacustrine and mudflat, and back to fluvial and eolian facies associations. A third transgressive cycle is represented by a change from eolian to alluvial fan and mudflat facies associations between 7568 and 7151 ft, and finally to fan delta and lacustrine facies associations between 5406 and 5395 ft.

These repetitive transgression and regression cycles that compose the rift sequences are probably controlled by the interplay of tectonism and climate. Each rift sequence, with sequence boundaries composed of flooding surfaces, starts after an episode of igneous extrusion. This clearly reflects the tectonic control on the basin evolution. As the tectonic adjustments were taking place, each tectonic pulse created accommodation, followed by subsequent sedimentation and subsidence, a pattern that is common in syn-rift successions (Martins-Neto and Catuneanu, 2010).

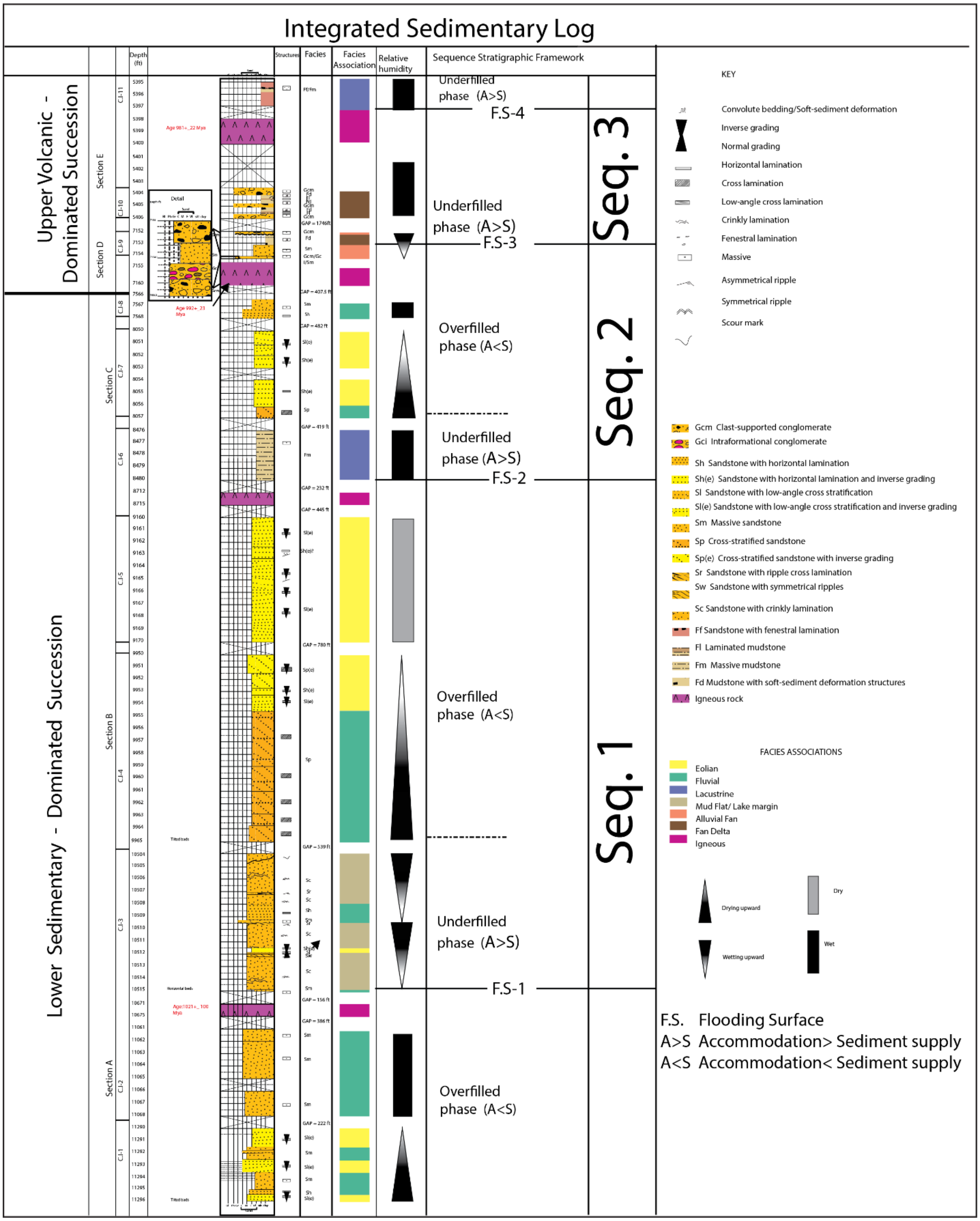


Figure 5.6 : Integrated sedimentary log with identified sequence of rift basin fill within NP#1.

In terms of sedimentary provenance in the rift basin, the overall composition of the studied samples has a higher amount of K-feldspar over plagioclase, suggesting alkaline plutonic and metamorphic rocks as the source for the sediments (Boggs, 2014), verified by the fact that plutonic and metamorphic rock fragments comprise the most abundant lithic fragments. Considering the compositional variations at different depth intervals (Figure-4.10 and 4.14), during rift evolution there seems to be a shift of sediment sources and transportation pathways.

The provenance changes in Section C, from uplifted continental block to dissected magmatic arc and transitional continental (Figure-4.14), and diversification in sediment composition from Section C onwards (Figure-4.10), suggests a re-arrangement of drainage basin and introduction of newer sources. The uplift and subsequent erosion of the faulted block provided sediments to the basin and it ultimately led to the subsidence. Also, the tectonic activities caused re-arrangement of drainage basins, as discussed in chapter 4, and coalescence of different pathways.

However, basin evolution and sedimentation are not solely controlled by the tectonic features. The pathways for bringing the sediments into the basin, as well as the climate that influences the weathering, transportation of the sediments, and facies, are equally important in terms of understanding the evolutionary history of the rift basin (Nichols and Uttamo, 2005). Therefore, considering the repetitive changes in the depositional environments, from subaqueous to subaerial, it appears that the tectonic cycles are superimposed by the effects of climate, which may be linked to relative sea-level changes. Eustatic changes are not significant in continental basins, such as the MRS, but it is evident that climate exerted significant control in facies analysis and, thus, sedimentation into the basin.

## 5.3 Correlation with other parts of MRS

Establishing a correlation between the different units of the Keweenawan Supergroup, *i.e.*, units deposited in different segments of MRS, is challenging because it resulted from an episodic event that not only comprised pulses controlled by allogenic factors, but also had variable intensity in the different segments (Stein et al., 2018). This spatial and temporal complexity resulted in the diachronous deposition of units in different environments. Better age data can be helpful in this matter, and several works have attempted to correlate the units deposited in different areas of the MRS (Anderson et al., 1987; Ojakangas et al., 2002). Figure-5.7 presents a correlation chart of units between different segments, based on age data gathered so far.

Since no geochronological data are available for the rift sedimentary deposits from the KS segment, K-Ar ages in volcanic rocks in the NP#1 well (Berendsen, 1997) were used to correlate the studied rocks with deposits in other rift segments. These ages indicate that the rift deposits in KS are coeval with post-rift successions elsewhere (Ojakangas, 2002). The ages of the volcanics in KS are similar to those of the Oronto and Bayfield Groups and their equivalents, identified as post-rift deposits (Ojakangas et al., 2002).

The development of MRS has been suggested to be episodic (Morey and Green, 1982; Malone et al., 2016). While the earliest igneous activity related to MRS began considerably before 1,110 ± 10 Ma (Wanless and Loveridge, 1978), the youngest igneous rock found in Noel Poersch#1 yielded an age of 992 ± 23 Ma. Considering these ages, it would be unlikely that the studied succession represents a syn-rift package, as it seems unacceptable to assume that the rifting process was active for about 100 Ma. Compared to younger rifts, such as the Miocene East African rift (Ebinger, 2005) and Oligocene Rio Grande rift (Chapin et al., 1994), it would be surprising if the MRS had been active as a rift for such a long time.

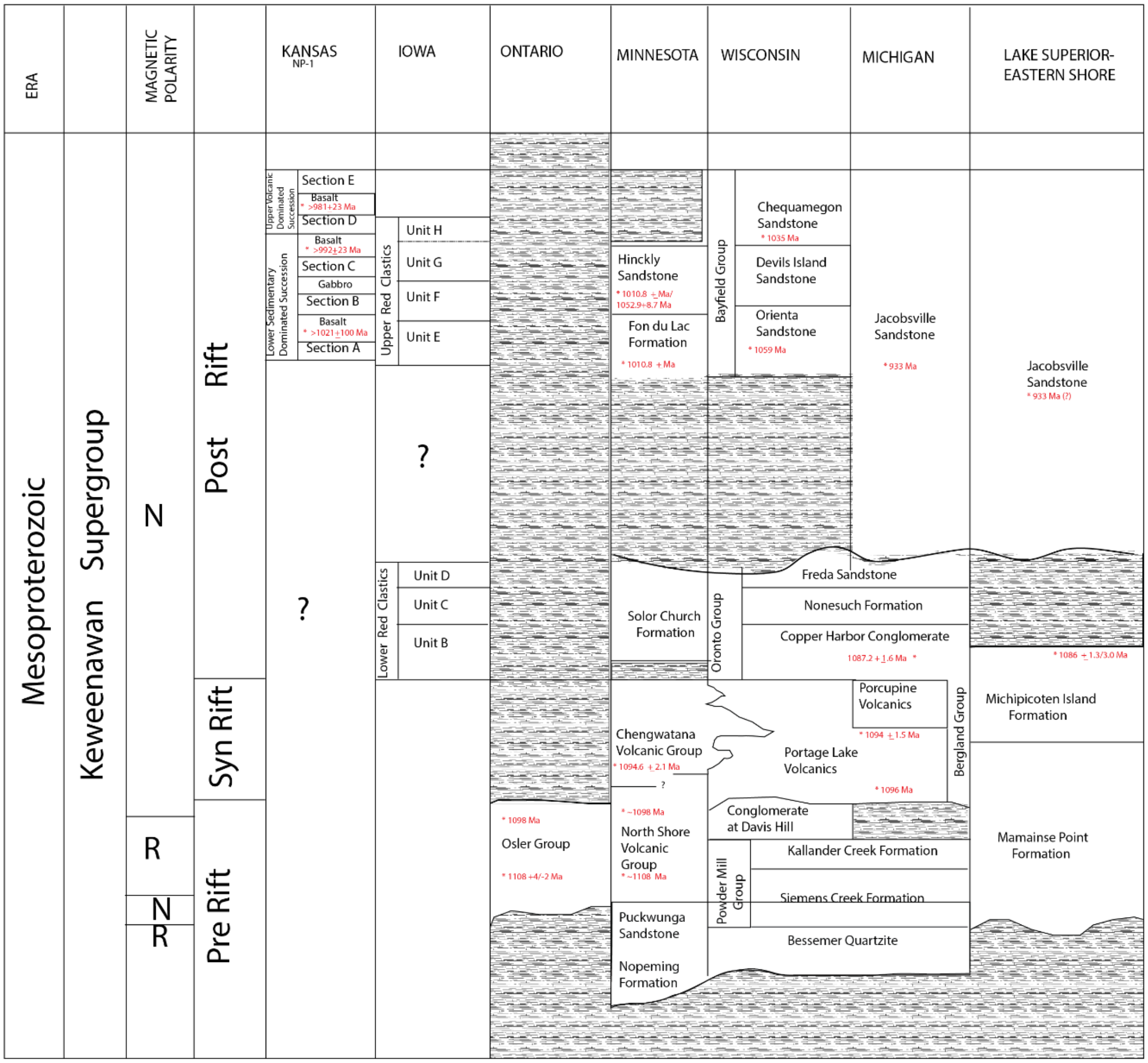


Figure 5.7 : Comparative stratigraphy of units that comprise the Keeweenawan Supergroup in different locations. Age data and stratigraphic nomenclature for the different locations compiled from Berendsen, 1997 (NP#1 KS), Anderson et al., 1987 (IA) and Ojakangas et al., 2002.

Another observation that is in accordance with a post-rift setting for the studied succession is the fact that the studied core samples have a higher percentage of plutonic relative to volcanic and sedimentary rock fragments, similar to what was reported for cuttings in NP#1 (Berendsen, 1997). Recurrent tectonic movements and subsequent erosion during syn-rift stages leads to increased accommodation and subsidence (Bosence, 1998), supplying near-source sediments from the uplifted blocks to the rift basin, which would result in syn-rift successions enriched in supracrustal rocks, the opposite of what was observed in NP#1.

On the other hand, the stacking pattern and the identified sequences (Figure-5.6) agrees with a syn-rift setting rather than post rift one. The identification of flooding surfaces indicative of subsidence (Bosence, 1998) and successive depositions suggests responses towards tectonic pulse. The repetitive occurrence ultimately leads to a coarsening-upward vertical stacking pattern as the rift continues to progress (Catuneanu, 2010). Such patterns are indicative of syn-rift successions, for example, Sopa-Brumadinho sequence, part of the syn-rift stage, Espinhaço Basin, Brazil (Martins-Neto, 1993).

Despite the correlation of post-rift successions based on geochronological data, the packages deposited in different segments of MRS are compositionally very different (Figure-5.7). While the samples from Lake Superior region are mostly litho-feldspathic (Ojakangas et al., 2002), the red bed clastics in M.G. Eischield#1 well from Iowa are arkosic-subarkosic (Anderson et al., 1987), and the studied samples from NP#1 are arkosic-lithic (Figure-5.8). Such variations are not uncommon in rift basins, considering that both basin geometry and basement lithology may vary from one place to the other. The composition of basement rocks plays a vital role, alongside climate and relief, thus controlling the composition of the basin infill (Nichols, 2009). The pre-rift basement rocks in Kansas include accredited Proterozoic arc terrane and granitoid from 1.76 to 1.6 Ga (Whitmeyer and Karlstrom, 2007), whereas rift segments further to the north (Lake Superior, Minnesota) sit on 2.5 Ga Archean crust. Variations in the compositional suite of basin infill in different rift segments, as noted on figure-5.8, may be reflecting differences in the pre-rift basement rocks.

Another difference between the post-rift successions across the MRS is the thickness of the volcanic-sedimentary units. The syn-rift succession of northern segments of MRS (Portage Lake Volcanics), where rifting was the most intense, contains a minor amount of interflow sedimentary packages, less than 3% of total syn-rift succession exposed in Houghton County, Michigan (24,750ft), while the sedimentary package in NP#1 in KS comprises more than 50% of the succession (total thickness 8454ft) (Berendsen, 1997), i.e. there was considerably less volcanism at this extreme southern end of the rift. Therefore, substantial differences were found in the rift succession in KS in comparison to other parts of the MRS, and without further data, it is not possible to determine with confidence what the relationships are between the different units, or even whether the studied succession in KS is syn- or post-rift.

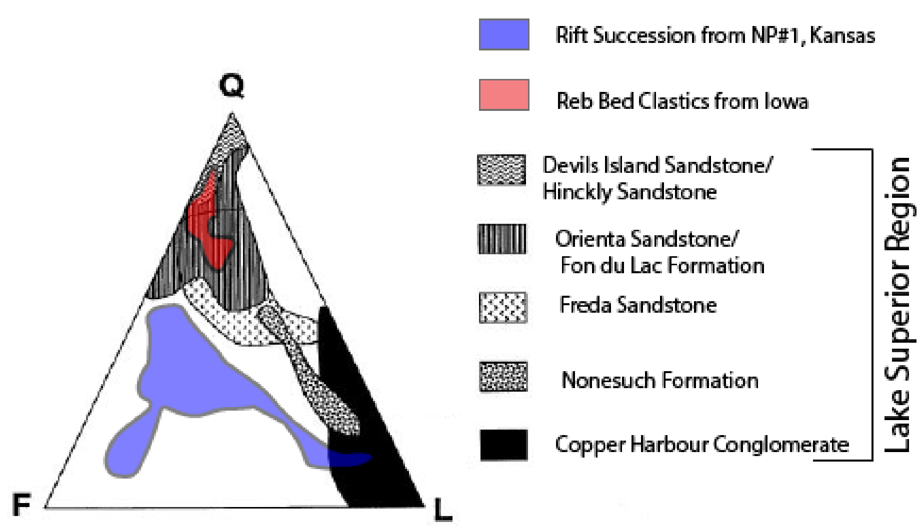


Figure 5.8 : Compositional ternary diagram comparing sandstones deposited in different rift segments of MRS. Data for units in Iowa (Red bed clastics) and Lake Superior region compiled from Anderson et al. (1987) and Ojakangas et al. (2002), respectively.

# Chapter 6 - Conclusion

In this study a depositional model and stratigraphic framework for the rift section of the MRS in Kansas have been proposed on the basis of detailed facies and provenance analysis of cores from the Noel Porsch #1 well.

Sixteen lithofacies are identified and grouped into six different facies associations (fluvial, eolian, mudflat/lake margin, lacustrine, alluvial fan, and fan delta). Overall, the studied succession comprises continental deposits laid down dominantly in alluvial and eolian settings, with the intermittent development of lacustrine systems. However, the lack of a significant amount of data due to the limited core retrieval impaired the ability to infer the extension and temporal changes in depositional environments throughout rift basin evolution.

Recognition of four flooding surfaces provides evidence for three distinct rift sequences, controlled by tectonic pulses in the rift basin. These tectonic pulses created accommodation that was followed by infilling of that accommodation. Superimposed on the tectonic phases, changing climate conditions resulted in recurrent dry and wet cycles. Therefore, the proposed depositional model and tectono-stratigraphic framework represent the interplay between tectonic and climatic controls.

Provenance analysis shows the sediment source to be of plutonic and high-grade metamorphic rocks, compared to minor sedimentary and volcanic contributions. This reflects a higher contribution of infracrustal source areas, such as uplifted basement blocks. No major changes in provenance were noticed throughout rift evolution, except a minor shift to transitional continental and magmatic arc, which eventually reverted to continental basement block. This could be due to re-arrangements of faulted blocks and variable proportions of axial vs. transversal input into the rift basin. Another possibility could be the variation in bedrock composition controlling the sediment source.

Overall, the available geochronological data suggests the rift succession in KS to be more compatible with post-rift successions elsewhere, whereas the tectono-stratigraphic framework and the upward increase in abundance of volcanics in the studied well in KS is typical of a syn-rift succession. At the moment, there is not enough evidence to rule out either possibility.

# References


Anderson, R. R., McCay, R. M., Berendsen, P., & Morey, G. B. (1987). Clastic rock associated with the Midcontinent Rift System North-Central USA. United States Geological Survey.

Arribas, J., Alonso, A., Mas, R., Tortosa, A., Rodas, M., Barrenechea, J. F., ... & Artigas, R. (2003). Sandstone petrography of continental depositional sequences of an intraplate rift basin: Western Cameros Basin (North Spain). Journal of sedimentary research, 73(2), 309-327.

Barr, D. (1987). Structural/stratigraphic models for extensional basins of half-graben type. Journal of Structural Geology, 9(4), 491–500.

Behrendt, J. C., Hutchinson, D. R., Lee, M., Thornber, C. R., Trehu, A., Cannon, W., & Green, A. (1990). GLIMPCE seismic reflection evidence of deep-crustal and upper-mantle intrusions and magmatic underplating associated with the Midcontinent Rift system of North America. Tectonophysics, 173(1-4), 595-615.

Berendsen, P. (1997). Tectonic evolution of the midcontinent rift system in Kansas. Geological Society of America Special Papers, 312, 235–241.

Boggs Jr, S. (2014). *Principles of sedimentology and stratigraphy*. Pearson Education.

Bose, P.K., Eriksson, P.G., Sarkar, S., Wright, D.T., Samanta, P., Mukhopadhyay, S., Mandal, S., Banerjee, S., Altermann, W., 2012. Sedimentation patterns duringthe Precambrian: a unique record? Mar. Petrol. Geol. 33, 34-68.

Bosence, D. (1998). Stratigraphic and sedimentological models of rift basins. In Sedimentation and Tectonics in Rift Basins Red Sea:-Gulf of Aden (pp. 9–25). Springer.

Bosworth, W. (1987). Off-axis volcanism in the Gregory rift, east Africa: Implications for models of continental rifting. Geology, 15(5), 397–400.

Bosworth, W., Lambiase, J., & Keisler, R. (1986). A new look at Gregory's rift: the structural style of continental rifting. Eos, Transactions American Geophysical Union, 67(29), 577–583.

Bott, M. (1992). Modelling the loading stresses associated with active continental rift systems. Tectonophysics, 215(1–2), 99–115.

Bridge, J. S., & Leeder, M. R. (1979). A simulation model of alluvial stratigraphy. Sedimentology, 26(5), 617-644.

Burov, E., & Cloetingh, S. A. P. L. (1997). Erosion and rift dynamics: new thermomechanical aspects of post-rift evolution of extensional basins. Earth and Planetary Science Letters, 150(1-2), 7-26.

Chapin, C. E., Cather, S. M., & Keller, G. R. (1994). Tectonic setting of the axial basins of the northern and central Rio Grande rift. *SPECIAL PAPERS-GEOLOGICAL SOCIETY OF AMERICA*, 5-5.

Collinson, J.D. (1996). Alluvial sediments.H.G Reading (Ed.), Sedimentary Environments: Processes, Facies and Stratigraphy, Blackwell Scientific Publications, Oxford, pp. 37-82.

Catuneanu, O., Galloway, W. E., Kendall, C. G. S. C., Miall, A. D., Posamentier, H. W., Strasser, A., & Tucker, M. E. (2011). Sequence stratigraphy: methodology and nomenclature. Newsletters on stratigraphy, 44(3), 173-245.

Craddock, C., Thiel, E. C., & Gross, B. (1963). A gravity investigation of the Precambrian of southeastern Minnesota and western Wisconsin. Journal of Geophysical Research, 68(21), 6015–6032.

De Ros, L.F., Goldberg, K., Abel, M., Victoreti, F., Mastella, M. & Castro, E. 2007. Advanced Acquisition and Management of Petrographic from Reservoir Rocks using PETROLEDGE®

System. *In*: AAPG ANNUAL CONVENTION AND EXHIBITION, 2007, Long Beach. *Expanded Abstracts*, p. 1-4.
Dickinson W.R. (1985) Interpreting Provenance Relations from Detrital Modes of Sandstones. In: Zuffa G.G. (eds) Provenance of Arenites. NATO ASI Series (Series C: Mathematical and Physical Sciences), vol 148. Springer, Dordrecht.
Dickson, J. A. D. (1965). A modified staining technique for carbonates in thin section. Nature, 205(4971), 587-587.
Ebinger, C. (2005). Continental break-up: The East African perspective. *Astronomy & Geophysics*, *46*(2), 2-16.
Elling, R. P., Stein, S., Stein, C. A., & Barklage, M. (2019). Unscrambling the Midcontinent Rift and Grenville Front in the eastern United States. AGU Fall Meeting 2019.
Eriksson, P.G., Condie, K.C., Tirsgaard, H., Mueller, W.U., Altermann, W., Miall, A.D., Aspler, L.B., Catuneanu, O., Chiarenzelli, J.R, 1998. Precambrian clastic sedimentation systems. Sedimentary Geology 120, 5-53.
Halls, H. C. (1978). The use of converging remagnetization circles in palaeomagnetism. Physics of the Earth and Planetary interiors, 16(1), 1-11.
Hawkesworth, C. J., Cawood, P. A., Dhuime, B., & Kemp, T. I. (2017). Earth's continental lithosphere through time. Annual review of earth and planetary sciences, 45, 169-198.
Hinze, W. J., Allen, D. J., Fox, A. J., Sunwood, D., Woelk, T., & Green, A. G. (1992). Geophysical investigations and crustal structure of the North American Midcontinent Rift system. Tectonophysics, 213(1–2), 17–32.
Ingersoll, R.V.; Bullard, T.F.; Ford, R.L.; Grimm, J.P.; Pickle, J.D.; Sares, S.W. 1984. The effect of grain size on detrital modes: a test of the Gazz|-Dickinson point-counting method. Journal of Sedimentary Petrology, v. 54, n. 1, p. 103-116.
James, N. P., & Dalrymple, R. W. (2010). Fácies models 4. Geological association of Canada Canada.
Jervey, M. T. (1988). Quantitative geological modeling of siliciclastic rock sequences and their seismic expression.
King, E. R., & Zietz, I. (1971). Aeromagnetic study of the midcontinent gravity high of central United States. Geological Society of America Bulletin, 82(8), 2187-2208.
Lam, C. K., & Yarger, H. L. (1989). State gravity map of Kansas. Geophysics in Kansas: Kansas Geological Survey, Bulletin, 226, 185-196.
Leeder, M., & Gawthorpe, R. (1987). Sedimentary models for extensional tilt-block/half-graben basins. Geological Society, London, Special Publications, 28(1), 139–152.
Malone, D.H., Stein, C.A., Craddock,J.P., Kley, J., Stein, S., and Malone, J.E.( 2016). Maximum depositional age of the Neoproterozoic Jacobsville Sandstone, Michigan: Implications for the evolution of the Midcontinent Rift: Geosphere, v. 12, no. 4, p. 1271–1282, doi:10.1130/GES01302.1.
Martins-Neto, M. A. (2000). Tectonics and sedimentation in a paleo/mesoproterozoic rift-sag basin (Espinhaço basin, southeastern Brazil). Precambrian Research, 103(3-4), 147-173.
Martins-Neto, M. A., & Catuneanu, O. (2010). Rift sequence stratigraphy. Marine and Petroleum Geology, 27(1), 247-253.
McBride, E. F. (1963). A classification of common sandstones. Journal of Sedimentary Research, 33(3), 664-669.

McCoy, S. W., Kean, J. W., Coe, J. A., Staley, D. M., Wasklewicz, T. A., & Tucker, G. E. (2010). Evolution of a natural debris flow: In situ measurements of flow dynamics, video imagery, and terrestrial laser scanning. Geology, 38(8), 735–738.

McSwiggen, P. L., Morey, G., & Chandler, V. W. (1987). New model of the midcontinent rift in eastern Minnesota and western Wisconsin. Tectonics, 6(6), 677–685.

Merk, G. P., & Jirsa, M. A. (1982). Provenance and tectonic significance of the Keweenawan interflow sedimentary rocks. Geology and Tectonics of the Lake Superior Basin. Edited by RJ Wold and WJ Hinze. Geological Society of America, Memoir, 156, 97–105.

Miall, A. D. (1977). Lithofacies types and vertical profile models in braided river deposits: a summary.

Miall, A.D. (1977). A review of the braided river depositional environment: Earth-Science Reviews, v. 13, p. 1–62.

Miall, A.D. (1978). Lithofacies types and vertical profile models in braided river deposits: a summary, in Miall, A.D., ed., Fluvial Sedimentology: Canadian Society of Petroleum Geologists, Memoir 5, p. 597–604.

Miall, A. D. (1985). Architectural-element analysis: a new method of facies analysis applied to fluvial deposits. Earth-Science Reviews, 22(4), 261–308.

Miall, A. D. (2006). Lithofacies. In The Geology of Fluvial Deposits (pp. 99-130). Springer, Berlin, Heidelberg.

Mineral Deposits of the Midcontinent Rift System. (n.d.) Retrieved from arcgis.com/apps/MapSeries/index.html?appid=6687aedec0c2452db15b85ea253fb842.

Morey, G. B., & Green, J. C. (1982). Status of the Keweenawan as a stratigraphic unit in the Lake Superior region. Geology and tectonics of the Lake Superior basin: Geological Society of America Memoir, 156, 15-26.

Nichols, G. (2009). Sedimentology and stratigraphy. John Wiley & Sons.

Nichols, G., & Uttamo, W. (2005). Sedimentation in a humid, interior, extensional basin: the Cenozoic Li Basin, northern Thailand. Journal of the Geological Society, 162(2), 333-347.

Nicholson, S. W., & Shirey, S. B. (1990). Midcontinent rift volcanism in the Lake Superior region: Sr, Nd, and Pb isotopic evidence for a mantle plume origin. Journal of Geophysical Research: Solid Earth, 95(B7), 10851-10868.

Ojakangas, R. W., & Dickas, A. B. (2002). The 1.1-Ga Midcontinent Rift System, central North America: sedimentology of two deep boreholes, Lake Superior region. Sedimentary Geology, 147(1–2), 13–36.

Ojakangas, R., Morey, G., & Green, J. (2001). The Mesoproterozoic midcontinent rift system, Lake Superior region, USA. Sedimentary Geology, 141, 421–442.

Paces, J. B., & Bell, K. (1989). Non-depleted sub-continental mantle beneath the Superior Province of the Canadian Shield: Nd-Sr isotopic and trace element evidence from Midcontinent Rift basalts. Geochimica et Cosmochimica Acta, 53(8), 2023–2035.

Reading, H.G. (1996). Sedimentary Environments: Processes, Facies & Stratigraphy (3rd ed), Black well scientific publications.

Schieber, J., Bose, P. K., Eriksson, P. G., Banerjee, S., Sarkar, S., Altermann, W., & Catuneanu, O. (Eds.). (2007). Atlas of microbial mat features preserved within the siliciclastic rock record. Elsevier.

Scott, R. W. (1966). New Precambrian (?) formation in Kansas. American Association of Petroleum Geologists Bulletin.

Serpa, L., Setzer, T., Farmer, H., Brown, L., Oliver, J., Kaufman, S., Steeples, D. W. (1984). Structure of the southern Keweenawan rift from COCORP surveys across the Midcontinent geophysical anomaly in northeastern Kansas. Tectonics, 3(3), 367–384.

Somanas, C., Knapp, R. W., Yarger, H. L., & Steeples, D. W. (1989). Geophysical model of the Midcontinent Geophysical Anomaly in northeastern Kansas. Kansas Geological Survey Bulletin, 226, 228.

Sønderholm, M., Tirsgaard, H., 1998. Proterozoic fluvial styles: response to changes in accommodation space (Rivieradal sandstones, eastern North Greenland). Sedimentary Geology 120, 257-274.

Soofi, M. A., & King, S. D. (2002). Post-rift deformation of the Midcontinent rift under Grenville tectonism. Tectonophysics, 359(3-4), 209-223.

Stein, S., Stein, C. A., Elling, R., Kley, J., Keller, G. R., Wysession, M. & Moucha, R. (2018). Insights from North America's failed Midcontinent Rift into the evolution of continental rifts and passive continental margins. Tectonophysics, 744, 403-421.

Suarez-Gonzalez, P., Benito, M. I., Quijada, I. E., Mas, R., & Campos-Soto, S. (2019). 'Trapping and binding': A review of the factors controlling the development of fossil agglutinated microbialites and their distribution in space and time. Earth-Science Reviews.

Tamrakar, N. K., Shrestha, P., & Maharjan, S. (2009). Facies association and depositional environment of fan-delta sequence in southwest Kathmandu Basin, Nepal. Bulletin of the Department of Geology, 12, 1-16.

Thiel, E. (1956). Correlation of gravity anomalies with the Keweenawan geology of Wisconsin and Minnesota. Geological Society of America Bulletin, 67(8), 1079-1100.

Wanless, R. K., RK, W., & WD, L. (1978). Rubidium-strontium Isotopic Age Studies, Report 2 (canadian Shield).

Woollard, G. P. (1943). Transcontinental gravitational and magnetic profile of North America and its relation to geologic structure. Bulletin of the Geological Society of America, 54(6), 747-790.

Xia, J., Sprowl, D. R., & Steeples, D. W. (1996). A model of Precambrian geology of Kansas derived from gravity and magnetic data. Computers & Geosciences, 22(8), 883-895.

Zuffa G.G. 1985. Optical analyses of arenites: influence of methodology on compositional results. *In:* Zuffa G.G. (ed.) *Provenance of Arenites*. NATO-ASI Series C. D. Reidel Pub. Co., 148, Dordrecht, The Netherlands, p. 165-168.

# Appendix A

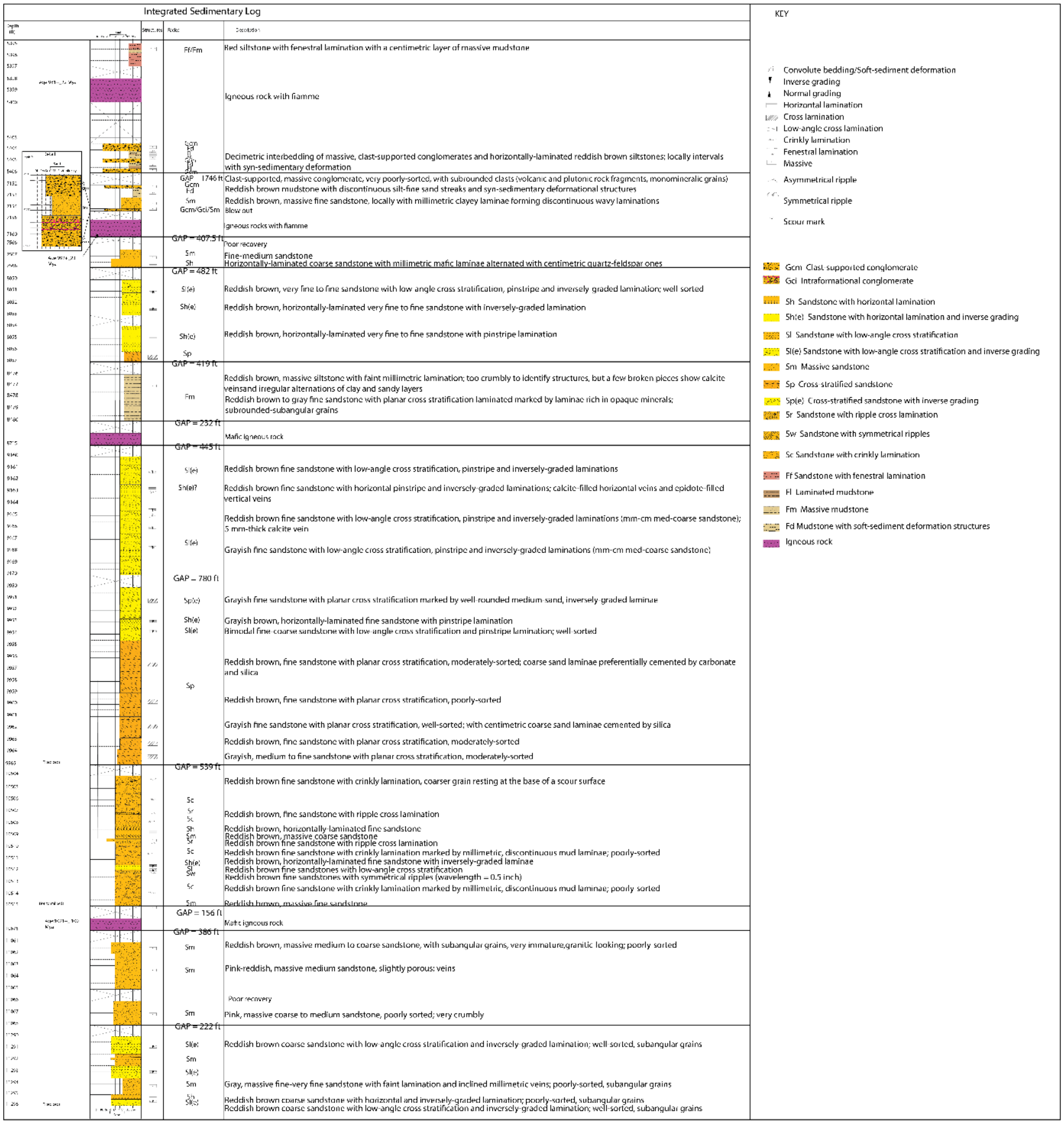

Integrated Sedimentary Log
KEY
Red siltstone with fenestral lamination with a centimetric layer of massive mudstone
Igneous rock with fiamme
Decimetric interbedding of massive, clast-supported conglomerates and horizontally-laminated reddish brown siltstones; locally intervals with syn-sedimentary deformation
Clast-supported, massive conglomerate, very poorly-sorted, with subrounded clasts (volcanic and plutonic rock fragments, monomineralic grains)
Reddish brown mudstone with discontinuous silt-fine sand streaks and syn-sedimentary deformational structures
Reddish brown, massive fine sandstone, locally with millimetric clayey laminae forming discontinuous wavy laminations
Igneous rocks with fiamme
GAP = 407.5 ft
Poor recovery
Fine-medium sandstone
Horizontally-laminated coarse sandstone with millimetric mafic laminae alternated with centimetric quartz-feldspar ones
GAP = 482 ft
Reddish brown, very fine to fine sandstone with low angle cross stratification, pinstripe and inversely graded lamination; well sorted
Reddish brown, horizontally-laminated very fine to fine sandstone with inversely-graded lamination
Reddish brown, horizontally-laminated very fine to fine sandstone with pinstripe lamination
GAP = 419 ft
Reddish brown, massive siltstone with faint millimetric lamination; too crumbly to identify structures, but a few broken pieces show calcite veinsand irregular alternations of clay and sandy layers
Reddish brown to gray fine sandstone with planar cross stratification laminated marked by laminae rich in opaque minerals; subrounded-subangular grains
GAP = 232 ft
Mafic igneous rock
GAP = 445 ft
Reddish brown fine sandstone with low-angle cross stratification, pinstripe and inversely-graded laminations
Reddish brown fine sandstone with horizontal pinstripe and inversely-graded laminations; calcite-filled horizontal veins and epidote-filled vertical veins
Reddish brown fine sandstone with low-angle cross stratification, pinstripe and inversely-graded laminations (mm-cm med-coarse sandstone); 5 mm-thick calcite vein
Grayish fine sandstone with low-angle cross stratification, pinstripe and inversely-graded laminations (mm-cm med-coarse sandstone)
GAP = 780 ft
Grayish fine sandstone with planar cross stratification marked by well-rounded medium sand, inversely graded laminae
Grayish brown, horizontally-laminated fine sandstone with pinstripe lamination
Bimodal fine-coarse sandstone with low-angle cross stratification and pinstripe lamination; well-sorted
Reddish brown, fine sandstone with planar cross stratification, moderately-sorted; coarse sand laminae preferentially cemented by carbonate and silica
Reddish brown, fine sandstone with planar cross stratification, poorly-sorted
Grayish fine sandstone with planar cross stratification, well-sorted; with centimetric coarse sand laminae cemented by silica
Reddish brown, fine sandstone with planar cross stratification, moderately-sorted
Grayish, medium to fine sandstone with planar cross stratification, moderately-sorted
GAP = 539 ft
Reddish brown fine sandstone with crinkly lamination, coarser grain resting at the base of a scour surface
Reddish brown, fine sandstone with ripple cross lamination
Reddish brown, horizontally-laminated fine sandstone
Reddish brown, massive coarse sandstone
Reddish brown fine sandstone with ripple cross lamination
Reddish brown fine sandstone with crinkly lamination marked by millimetric, discontinuous mud laminae; poorly-sorted
Reddish brown, horizontally-laminated fine sandstone with inversely-graded laminae
Reddish brown fine sandstones with low-angle cross stratification
Reddish brown fine sandstones with symmetrical ripples (wavelength = 0.5 inch)
Reddish brown fine sandstone with crinkly lamination marked by millimetric, discontinuous mud laminae; poorly sorted
Reddish brown, massive fine sandstone
GAP = 156 ft
Mafic igneous rock
GAP = 386 ft
Reddish brown, massive medium to coarse sandstone, with subangular grains, very immature,granitic looking; poorly sorted
Pink-reddish, massive medium sandstone, slightly porous; veins
Poor recovery
Pink, massive coarse to medium sandstone, poorly sorted; very crumbly
GAP = 222 ft
Reddish brown coarse sandstone with low-angle cross stratification and inversely graded lamination; well sorted, subangular grains
Gray, massive fine-very fine sandstone with faint lamination and inclined millimetric veins; poorly-sorted, subangular grains
Reddish brown coarse sandstone with horizontal and inversely-graded lamination; poorly-sorted, subangular grains
Reddish brown coarse sandstone with low-angle cross stratification and inversely-graded lamination; well-sorted, subangular grains
Convolute bedding/Soft-sediment deformation
Inverse grading
Normal grading
Horizontal lamination
Cross lamination
Low-angle cross lamination
Crinkly lamination
Fenestral lamination
Massive
Asymmetrical ripple
Symmetrical ripple
Scour mark
Gcm Clast supported conglomerate
Gci Intraformational conglomerate
Sh Sandstone with horizontal lamination
Sh(e) Sandstone with horizontal lamination and inverse grading
Sl Sandstone with low-angle cross stratification
Sl(e) Sandstone with low-angle cross stratification and inverse grading
Sm Massive sandstone
Sp Cross stratified sandstone
Sp(e) Cross-stratified sandstone with inverse grading
Sr Sandstone with ripple cross lamination
Sw Sandstone with symmetrical ripples
Sc Sandstone with crinkly lamination
Ff Sandstone with fenestral lamination
Fl Laminated mudstone
Fm Massive mudstone
Fd Mudstone with soft-sediment deformation structures
Igneous rock

# Appendix B

| | CI#1 | | | | CI#2 | | CI#3 | | | | CI#4 | | | | CI#5 | | CI#6 | CI#7 | | CI#8 | CI#9 | | | | CI#10 | | CI#111 |
|---|---|---|---|---|---|---|---|---|---|---|---|---|---|---|---|---|---|---|---|---|---|---|---|---|---|---|---|
| Depth (ft) | 11296 | 11295 | 11293. | 11290 | 11063.5 | 11061 | 10512 | 10515 | 10510 | 10509 | 9962 | 9957 | 9954 | 9951 | 9170 | 9164.7 | 8480 | 8056.6 | 8053.2 | 7568 | 7154.2 | 7154 | 7153 | 7152 | 5406 | 5404.2 | 5396 |
| Facies | Sle | Sh | Sm-Sle | Sle | Sm | Sm | She | Sc | Sc | Sc | Sp | Sp | Sle | Spe | Sle | She | Fm | She | She | Sh | Sm | Gci | Fd | Gcm | Gcm | Fl-Fd | Ff |
| Modal grain size | 0.28 | 0.104 | 0.8 | 0.15 | 0.69998 | 0.73 | 0.43 | 0.18 | 0.34 | 0.2099 | 0.33 | 0.23194 | 0.2 | 0.43999 | 0.2399 | 0.14 | 0.0799 | 0.23 | 0.25999 | 1.51997 | 0.2 | 0.1969 | 0.0189 | 5.86 | 5.86 | 0.20997 | 0.0299 |
| Numerical sorting | 0.6 | 1 | 1 | 0.6 | 0.6 | 0.6 | 0.6 | 0.6 | 0.6 | 0.4 | 0.6 | 0.6 | 1 | 0.6 | 1 | 0.6 | 0.4 | 0.4 | 0.6 | 0.6 | 2.2 | 1 | 0.4 | 2.2 | 2.2 | 0.6 | 1 |
| Sorting | Moderately | Poorly | Poorly | Moderately | Moderately | Moderately | Moderately | Moderately | Moderately | Well | Moderately | Moderately | Poorly | Moderately | Poorly | Moderately | Well | Well | Moderately | Moderately | Very poorl | Poorly | Well | Very poorl | Very poorl | Moderately | Poorly |
| Extrabasinal constituents | | | | | | | | | | | | | | | | | | | | | | | | | | | |
| Detrital quartz | 35 | 18 | 15.333 | 24.333 | 28.666 | 7.666 | 24.666 | 22.666 | 23.333 | 25 | 24 | 31.333 | 26.666 | 30.666 | 30 | 24.999 | 34.666 | 30.666 | 30.333 | 28 | 11.333 | 14.666 | 7.666 | 9.333 | 11.333 | 15.333 | 19.666 |
| Detrital feldspar | 31.666 | 11.333 | 22 | 34.666 | 27.666 | 46 | 39 | 30 | 40.666 | 33 | 31.666 | 27.666 | 33 | 33.666 | 29.333 | 32 | 21.666 | 26.666 | 23.333 | 29.333 | 10 | 11.333 | 6.666 | 14.666 | 9.333 | 14 | 17.333 |
| Total K- | 22.67 | 7.67 | 17.33 | 27.67 | 22.33 | 32.34 | 30.34 | 24 | 30.33 | 25 | 26.34 | 21.34 | 25.34 | 27 | 22.33 | 24.34 | 17.33 | 20 | 17.66 | 23.33 | 7.33 | 6.66 | 5.34 | 10.33 | 5.67 | 11.33 | 13.33 |
| Total plagioclas | 9 | 3.67 | 4.67 | 7 | 5.33 | 13.67 | 8.67 | 6 | 10.33 | 8 | 5.33 | 6.33 | 7.67 | 6.67 | 7 | 7.67 | 4.33 | 6.67 | 5.67 | 6 | 2.67 | 4.67 | 1.33 | 4.33 | 3.67 | 2.67 | 4 |
| Lithics | 9.333 | 21.999 | 9.665 | 21.998 | 9.999 | 10.333 | 9.333 | 13.998 | 13.999 | 11.999 | 22.666 | 12.665 | 18.999 | 11.333 | 16 | 11.332 | 5.666 | 18.666 | 23.332 | 30.332 | 11.333 | 3.999 | 1.332 | 49.332 | 64.665 | 8.333 | 0.666 |
| Metamorp | 0 | 1.333 | 0.666 | 2.333 | 1.333 | 0 | 0 | 5.666 | 1.666 | 3 | 5 | 3.333 | 1 | 1 | 5 | 0.333 | 3 | 7.333 | 13 | 9.333 | 2.333 | 0 | 0.333 | 4.666 | 1.333 | 0 | 0.333 |
| Plutonic | 8 | 17.333 | 8.333 | 17.333 | 8.666 | 10.333 | 8.333 | 7.666 | 10.333 | 7.666 | 16.333 | 7.333 | 16.333 | 9 | 11 | 6.666 | 2.333 | 7 | 7.666 | 20.666 | 7 | 1.666 | 0.666 | 43 | 61.666 | 8.333 | 0.333 |
| Volcanic | 1.333 | 3.333 | 0.666 | 0.666 | 0 | 0 | 1 | 0.666 | 2 | 1.333 | 1.333 | 1.666 | 1.666 | 1.333 | 0 | 4.333 | 0.333 | 4.333 | 2.666 | 0.333 | 2 | 2.333 | 0.333 | 1.666 | 1.666 | 0 | 0 |
| Sediment | 0 | 0 | 0 | 1.666 | 0 | 0 | 0 | 0 | 0 | 0 | 0 | 0.333 | 0 | 0 | 0 | 0 | 0 | 0 | 0 | 0 | 0 | 0 | 0 | 0 | 0 | 0 | 0 |
| Opaque minerals | 4 | 2 | 0.67 | 2.33 | 0 | 4.67 | 1.33 | 2.67 | 0.33 | 4 | 0 | 0.33 | 1 | 0.33 | 3.33 | 0 | 2.33 | 1.33 | 0.67 | 0.67 | 0.67 | 0.33 | 2.33 | 1 | 1.67 | 2.67 | 8 |
| Heavy minerals | 0 | 0.33 | 3.66 | 1 | 0 | 0.33 | 1.33 | 3.32 | 0.33 | 0.33 | 0 | 0.33 | 0 | 0 | 0 | 0.33 | 0.33 | 0 | 0 | 0 | 0.33 | 0 | 0.66 | 0.33 | 0 | 0 | 0.33 |

| | Diagenetic constituents | | | | | | | | | | | | | | | | | | | | | | | | | | |
|---|---|---|---|---|---|---|---|---|---|---|---|---|---|---|---|---|---|---|---|---|---|---|---|---|---|---|---|
| Total albite | 3 | 0 | 0.33 | 3 | 10.33 | 6.67 | 5.99 | 2.33 | 3.64 | 5.33 | 4.99 | 7.34 | 2.67 | 3 | 3 | 2.33 | 1.34 | 1.33 | 4.66 | 2.34 | 0 | 2 | 0 | 5.67 | 2.67 | 0 | 1 |
| Total calcite | 0.33 | 1.66 | 0.33 | 1.66 | 0 | 0.67 | 0.33 | 0 | 0 | 0 | 1 | 1.33 | 0 | 1.33 | 0.33 | 8 | 0 | 1.67 | 1 | 0 | 16.34 | 10 | 0.33 | 1 | 0 | 0 | 1 |
| Total epidote | 0 | 0.33 | 0 | 0 | 0 | 0 | 0 | 0 | 0 | 0 | 0.33 | 0.33 | 1.66 | 0 | 0.67 | 0.33 | 0.67 | 2 | 2 | 0.33 | 3.33 | 2.32 | 0 | 7.99 | 0.66 | 1.67 | 1 |
| Total Fe Oxide//H | 0 | 0 | 0 | 0 | 0 | 0 | 0 | 0 | 0 | 0 | 0 | 0 | 0 | 0 | 0 | 0 | 8 | 0 | 0 | 0 | 1.33 | 10.68 | 33.67 | 0.33 | 3 | 38.33 | 30.66 |
| Total illite | 1.33 | 7 | 5.67 | 2.66 | 0 | 0 | 2 | 3.99 | 0 | 0.99 | 0.66 | 5.34 | 6.67 | 0.67 | 1.33 | 0 | 0.67 | 1.33 | 0.33 | 1.33 | 0 | 0 | 0 | 0.33 | 0 | 0 | 0 |
| Total Ti minerals | 0 | 0 | 0 | 0 | 0 | 0 | 0 | 0 | 0 | 1 | 1.33 | 0.67 | 1 | 0.33 | 3.99 | 1.33 | 2.67 | 1.33 | 0 | 0.67 | 1 | 16 | 0 | 0.33 | 0 | 0 | 0 |